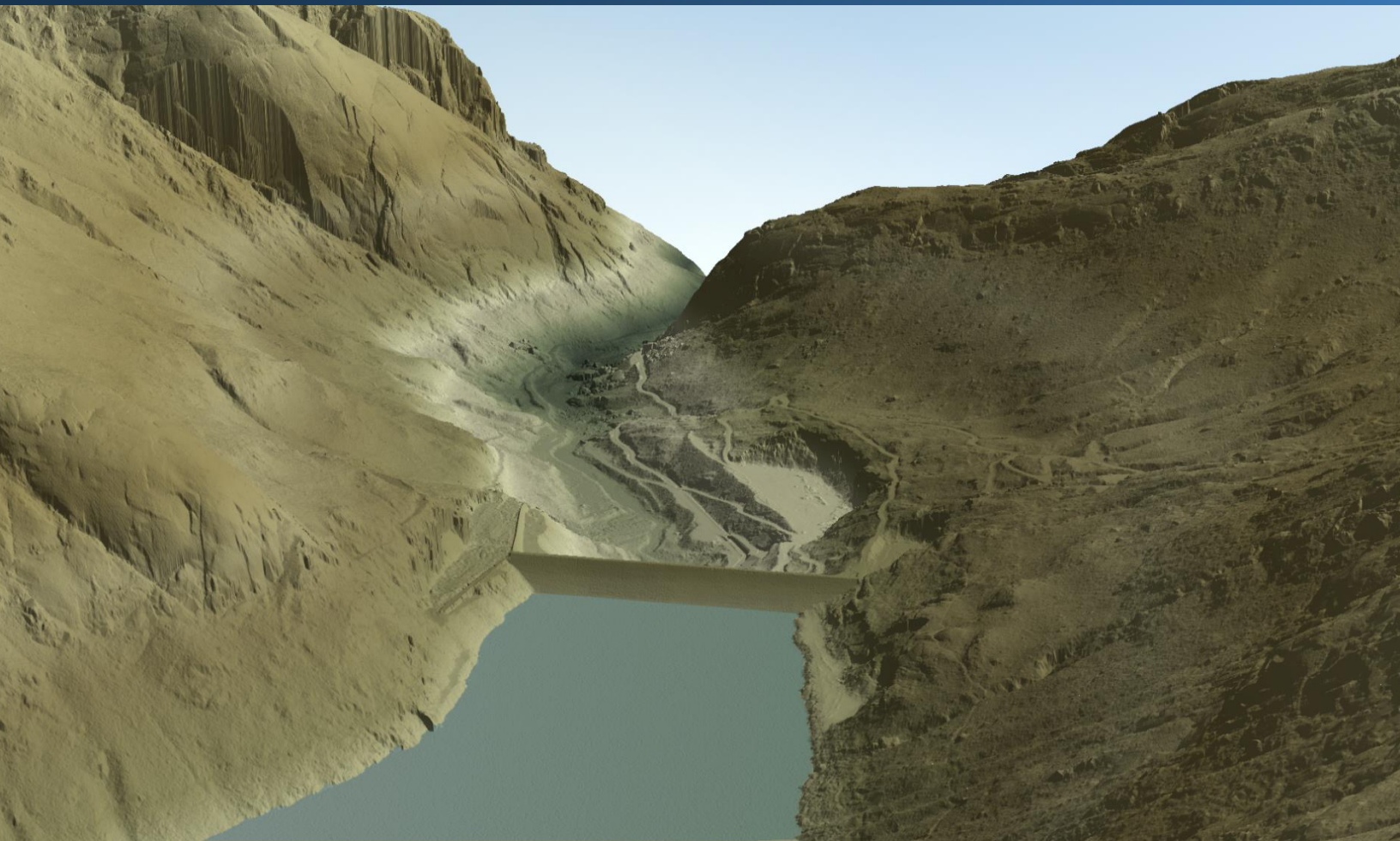


October 2, 2015



USFS Pacific Region 5 LiDAR

Technical Data Report



Carlos Ramirez

USDA Forest Service, Information Management
Region 5 Remote Sensing Laboratory
3237 Peacekeeper Way, Suite 201
McClellan, CA 95652
PH: 916-640-1275



QSI Environmental

517 SW 2nd St., Suite 400
Corvallis, OR 97333
PH: 541-752-1204

TABLE OF CONTENTS

| | |
|---|----|
| INTRODUCTION | 1 |
| Deliverable Products | 3 |
| ACQUISITION | 5 |
| Planning..... | 5 |
| Airborne Survey..... | 6 |
| LiDAR..... | 6 |
| Ground Control..... | 10 |
| Monumentation | 10 |
| Ground Survey Points (GSPs)..... | 12 |
| PROCESSING | 15 |
| LiDAR Data..... | 15 |
| RESULTS & DISCUSSION..... | 17 |
| LiDAR Density | 17 |
| LiDAR Accuracy Assessments | 24 |
| LiDAR Absolute Accuracy..... | 24 |
| LiDAR Vertical Relative Accuracy..... | 28 |
| CERTIFICATIONS | 30 |
| SELECTED IMAGES..... | 31 |
| GLOSSARY | 33 |
| APPENDIX A: ACCURACY CONTROLS | 34 |
| APPENDIX B: DENSITY RESULTS..... | 35 |
| APPENDIX C: ABSOLUTE ACCURACY RESULTS | 45 |
| APPENDIX D: RELATIVE ACCURACY RESULTS..... | 55 |

Cover Photo: View looking west over Salt Springs Reservoir. The image was created from a gridded LiDAR surface colored by elevation and overlaid with the 3D LiDAR point cloud.

INTRODUCTION

View looking southwest over the town of Strawberry, California. The image was created from a gridded LiDAR surface and overlaid with the 3D LiDAR point cloud and NAIP imagery.



In September 2014, Quantum Spatial (QSI) was contracted by the United States Forest Service (USFS) to collect Light Detection and Ranging (LiDAR) data in the fall of 2014 and spring of 2015 for the USFS Pacific Region 5 sites in California. Data were collected to aid USFS in assessing the topographic and geophysical properties of the study area to support ecological restoration planning and to assess existing conditions of area forests.

This report accompanies the final delivery of LiDAR data and documents contract specifications, data acquisition procedures, processing methods, and analysis of the final dataset including LiDAR accuracy and density. QSI provided two prior deliveries which are noted in Table 1. Acquisition dates and acreage of individual areas of interest (AOI) are shown in Table 1, a complete list of contracted deliverables provided to USFS are shown in Table 2, and the project extents are shown in Figure 1.

Table 1: Acquisition dates, acreage, and data types collected on the USFS Pacific Region 5 sites

| USFS Pacific Region 5 Project Sites | | | |
|--|--|-------------|--|
| Delivery | Project Sites | Total Acres | Acquisition Dates |
| Delivery 1, Sent to USFS on 02/13/2015 | Indiana Summit | 1,404 | 10/06/2014 |
| Delivery 2, Sent to USFS on 04/03/2015 | East Fork Scott River | 32,336 | 10/28/2014, 11/03/2014, 11/05/2014 |
| | Lower Elk Creek | 4,678 | 10/12/2014 |
| | Pendola | 6,446 | 10/05/2014 |
| | Squaw Creek | 3,235 | 10/09/2014 |
| | Stanislaus – Tuolumne Experimental Forest | 2,171 | 10/18/2014 |
| | Sugar Creek | 13,980 | 10/13/2014, 10/19/2014, 10/27/2014, 10/28/2014 |
| | Van Vleck Meadow | 7,199 | 10/07/2014 |
| Delivery 3, Sent to USFS on 10/02/2015 | Freds Fire | 156,392 | 10/16/2014 – 10/20/2014, 10/23/2014- 10/24/2014, 10/26/2014 – 10/29/2014, 11/2/2014, 11/5/2014, 11/8/2014 – 11/11/2014, 11/14/2014 – 11/19/2014, 11/21/2014, 11/23/2014, 11/26/2014 – 11/27/2014, 11/30/2014, 05/19/2015 – 05/21/2015, 05/31/2015, 06/02/2015- 06/03/2015 |
| | Power Fire | 114,195 | 11/23/2014-11/24/2014, 04/26/2015- 04/28/2015, 05/09/2015-05/13/2015, 05/16/2015, 05/21/2015, 05/28/2015- 06/05/2015 |

Deliverable Products

Table 2: Products delivered to USFS for the USFS Pacific Region 5 sites

| USFS Pacific Region 5 Products Projection: UTM Zone 10 North* Horizontal Datum: NAD83 (CORS96) Vertical Datum: NAVD88 (GEOID03) Units: Meters | |
|--|--|
| Points | LAS v 1.2 <ul style="list-style-type: none"> All Returns (.laz compressed) |
| Rasters | 1.0 Meter ENVI .dat files <ul style="list-style-type: none"> Bare Earth Model (1/4 USGS quads) Highest Hit Model (1/4 USGS quads) 0.5 Meter ENVI .dat files <ul style="list-style-type: none"> Normalized Intensity Images (1/4 USGS quads) |
| Vectors | Shapefiles (*.shp) <ul style="list-style-type: none"> Site Boundary LiDAR Tile Index (1/100th USGS quads) DEM Tile Index (1/4 USGS quads) Smooth Best Estimate Trajectory (SBETs) Flightline Swaths |

**The Indiana Summit AOI was projected in UTM Zone 11 North.*

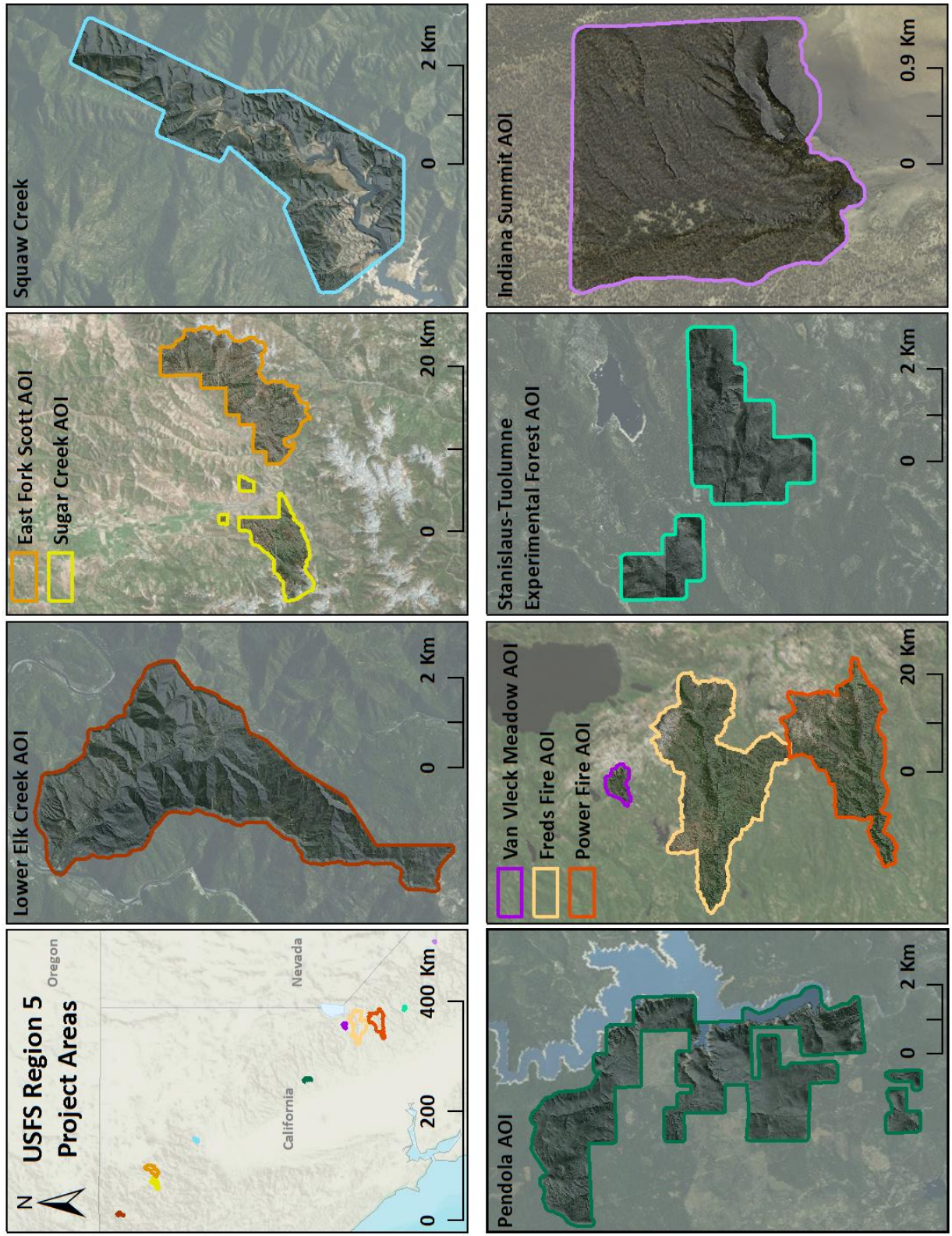


Figure 1: Location map of the USFS Pacific Region 5 sites in California

This picture shows a QSI base station set up within the Power Fire AOI of the USFS Region 5 Project Area.



Planning

In preparation for data collection, QSI reviewed the project area and developed a specialized flight plan to ensure complete coverage of the USFS Pacific Region 5 LiDAR study area at the target point density of ≥ 8.0 points/m². Acquisition parameters including orientation relative to terrain, flight altitude, pulse rate, scan angle, and ground speed were adapted to optimize flight paths and flight times while meeting all contract specifications.

Factors such as satellite constellation availability and weather windows must be considered during the planning stage. Any weather hazards or conditions affecting the flights were continuously monitored due to their potential impact on the daily success of airborne and ground operations. QSI flight and field crews ran into such weather related issues as strong winds and snow in higher elevations. Due to these issues and the large size of the Pacific Region 5 project (342,036 total acres), airborne LiDAR acquisition occurred between October 2014 and June 2015. In addition, logistical considerations including private property access and potential air space restrictions were reviewed.

Airborne Survey

LiDAR

The LiDAR survey was accomplished using Leica ALS50 and ALS70 systems. Table 3 and Table 4 summarize the settings used to yield an average pulse density of ≥ 8 pulses/m² over the USFS Pacific Region 5 project area. The Leica ALS50 laser system records up to four range measurements (returns) per pulse and the Leica ALS70 laser system can record unlimited range measurements (returns) per pulse, but typically does not record more than 5. It is not uncommon for some types of surfaces (e.g., dense vegetation or water) to return fewer pulses to the LiDAR sensor than the laser originally emitted. The discrepancy between first return and overall delivered density will vary depending on terrain, land cover, and the prevalence of water bodies. All discernible laser returns were processed for the output dataset.

Table 3: ALS70 Acquisition Parameters

| LiDAR Survey Settings & Specifications | | | | |
|--|--|--|--|--|
| Sensor | ALS70 | ALS70 | ALS70 | ALS70 |
| AOI | Power Fire, Freds Fire | Power Fire | Power Fire | Power Fire, Freds Fire |
| Acquisition Dates | See Table 1 | See Table 1 | See Table 1 | See Table 1 |
| Aircraft Used | Piper Navajo, or Cessna Caravan | Piper Navajo, or Cessna Caravan | Partenavia | Cessna Caravan |
| Survey Altitude (AGL) | varies | varies | varies | varies |
| Target Pulse Rate | 220kHz | 198kHz | 195kHz | 220kHz |
| Pulse Mode | Single Pulse in Air (SPiA) | Single Pulse in Air (SPiA) | Single Pulse in Air (SPiA) | Single Pulse in Air (SPiA) |
| Laser Pulse Diameter | 23cm - 30cm | 28cm - 34cm | 28 cm - 32 cm | 23cm - 30cm |
| Mirror Scan Rate | 54.0 Hz | 41.1Hz | 41.0 Hz | 59.9 Hz |
| Field of View | 30° | 30° | 30° | 30° |
| GPS Baselines | ≤ 13 nm | ≤ 13 nm | ≤ 13 nm | ≤ 13 nm |
| GPS PDOP | ≤ 3.0 | ≤ 3.0 | ≤ 3.0 | ≤ 3.0 |
| GPS Satellite Constellation | ≥ 6 | ≥ 6 | ≥ 6 | ≥ 6 |
| Maximum Returns | Unlimited, but typically not more than 5 | Unlimited, but typically not more than 5 | Unlimited, but typically not more than 5 | Unlimited, but typically not more than 5 |
| Intensity | 8-bit | 8-bit | 8-bit | 8-bit |
| Resolution/Density | Average 8 pulses/m2 | Average 8 pulses/m2 | Average 8 pulses/m2 | Average 8 pulses/m2 |
| Accuracy | $RMSE_z \leq 15$ cm | $RMSE_z \leq 15$ cm | $RMSE_z \leq 15$ cm | $RMSE_z \leq 15$ cm |

Table 4: ALS50 Acquisition Parameters

| LiDAR Survey Settings & Specifications | | | | |
|--|----------------------------|---|----------------------------|----------------------------|
| Sensor | ALS 50 | ALS 50 | ALS 50 | ALS 50 |
| AOI | East Fork Scott River | Indiana Summit, Pendola, Squaw Creek, ST Experimental Forest, Van Vleck Meadows | Lower Elk Creek | Sugar Creek |
| Acquisition Dates | See Table 1 | See Table 1 | See Table 1 | See Table 1 |
| Aircraft Used | Cessna Caravan | Cessna Caravan | Cessna Caravan | Cessna Caravan |
| Survey Altitude (AGL) | 900m | 900m | Varies | 900m |
| Target Pulse Rate | 106 kHz | 106 kHz | 106 kHz | 106 kHz |
| Pulse Mode | Single Pulse in Air (SPiA) | Single Pulse in Air (SPiA) | Single Pulse in Air (SPiA) | Single Pulse in Air (SPiA) |
| Laser Pulse Diameter | 21 cm | 21 cm | 20 cm - 23cm | 21 cm |
| Mirror Scan Rate | 66.3 Hz | 56.0 Hz | 54.0 Hz | 52.0 Hz |
| Field of View | 26° | 26° | 28° | 30° |
| GPS Baselines | ≤13 nm | ≤13 nm | ≤13 nm | ≤13 nm |
| GPS PDOP | ≤3.0 | ≤3.0 | ≤3.0 | ≤3.0 |
| GPS Satellite Constellation | ≥6 | ≥6 | ≥6 | ≥6 |
| Maximum Returns | 4 | 4 | 4 | 4 |
| Intensity | 8-bit | 8-bit | 8-bit | 8-bit |
| Resolution/Density | Average 8 pulses/m2 | Average 8 pulses/m2 | Average 8 pulses/m2 | Average 8 pulses/m2 |
| Accuracy | RMSEZ ≤ 15 cm | RMSEZ ≤ 15 cm | RMSEZ ≤ 15 cm | RMSEZ ≤ 15 cm |

All areas were surveyed with an opposing flight line side-lap of ≥50% (≥100% overlap) in order to reduce laser shadowing and increase surface laser painting. To accurately solve for laser point position (geographic coordinates x, y and z), the positional coordinates of the airborne sensor and the attitude of the aircraft were recorded continuously throughout the LiDAR data collection mission. Position of the aircraft was measured twice per second (2 Hz) by an onboard differential GPS unit, and aircraft attitude was measured 200 times per second (200 Hz) as pitch, roll and yaw (heading) from an onboard inertial measurement unit (IMU). To allow for post-processing correction and calibration, aircraft and sensor position and attitude data are indexed by GPS time.

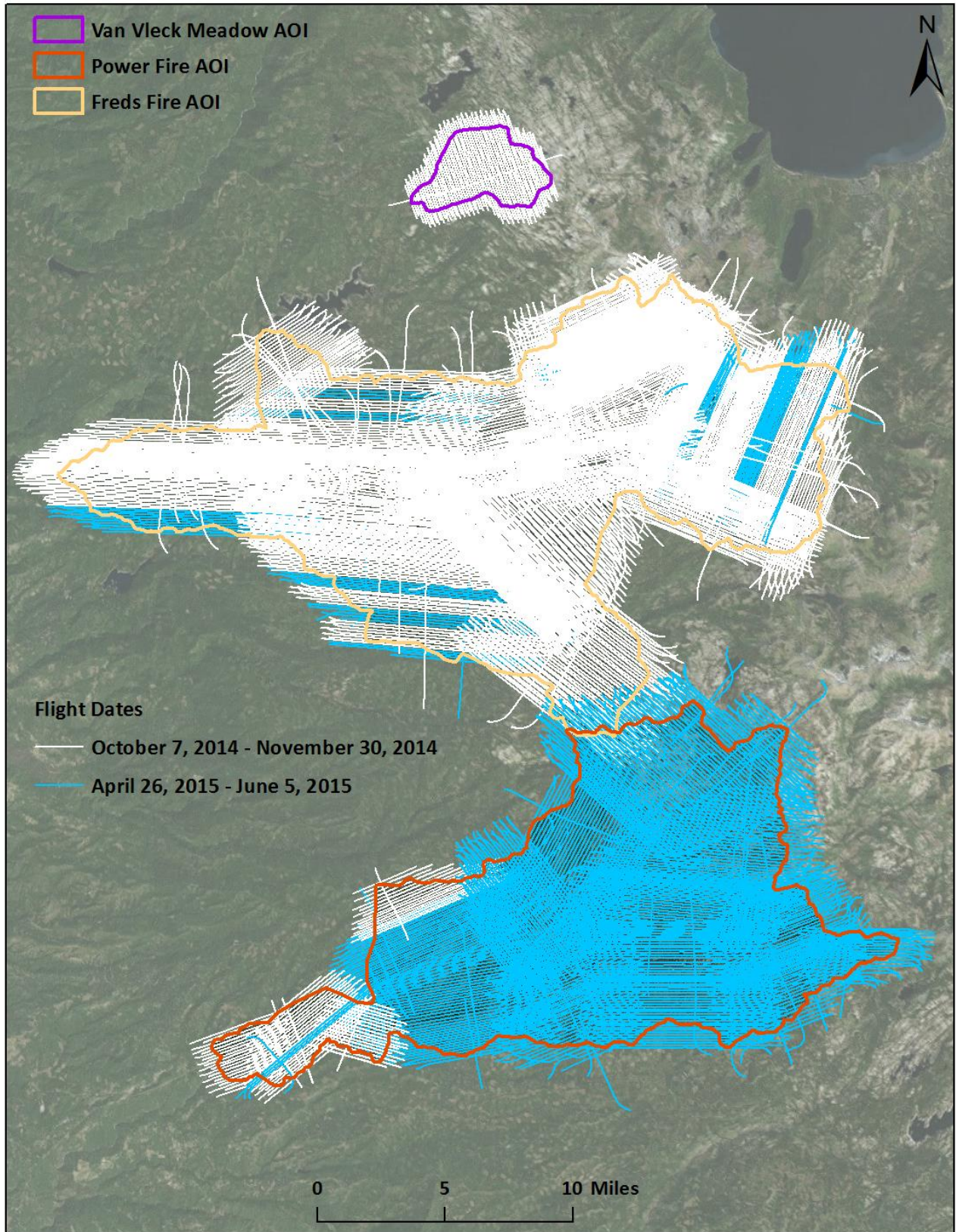


Figure 2: Flightline Index Map I

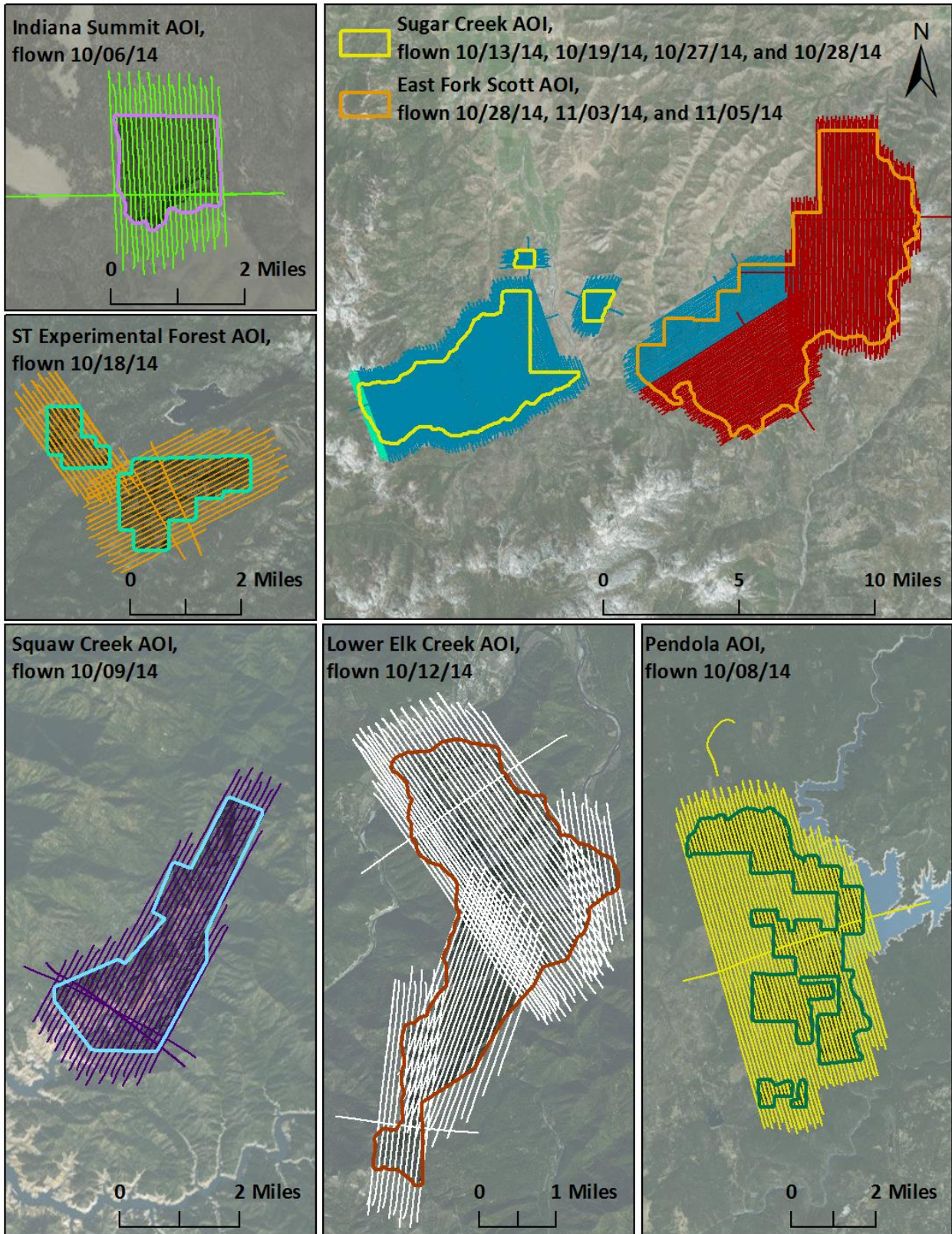


Figure 3: Flightline Index Map II

Ground Control

Ground control surveys, including monumentation and ground survey points (GSPs), were conducted to support the airborne acquisition. Ground control data were used to geospatially correct the aircraft positional coordinate data and to perform quality assurance checks on final LiDAR data.



*QSI-Established monument
SUGAR 01*

Monumentation

The spatial configuration of ground survey monuments provided redundant control within 13 nautical miles of the mission areas for LiDAR flights. Monuments were also used for collection of ground survey points using real time kinematic (RTK) and post processed kinematic (PPK) survey techniques.

Monument locations were selected with consideration for satellite visibility, field crew safety, and optimal location for GSP coverage. QSI utilized 14 existing monuments and established 18 new monuments for the USFS Pacific Region 5 LiDAR project (Table 5, Figure 4, Figure 5). New monumentation was set using 5/8" x 30" rebar topped with stamped 2" aluminum caps. QSI's professional land surveyor, Chris Glantz (CAPLS#8850) oversaw and certified the establishment of all monuments.

Table 5: Monuments established for the USFS Pacific Region 5 acquisition. Coordinates are on the NAD83 (CORS96) datum, epoch 2002.00

| Monument ID | Latitude | Longitude | Ellipsoid (meters) |
|---------------|-------------------|---------------------|--------------------|
| AF8159 | 40° 48' 26.66191" | -122° 19' 18.42826" | 393.276 |
| CDOT_2-3 | 41° 18' 05.95308" | -122° 44' 29.44858" | 1231.120 |
| DF4528 | 41° 48' 22.55258" | -123° 22' 03.24961" | 311.473 |
| DF5239 | 41° 18' 47.87434" | -122° 45' 11.58429" | 988.790 |
| DF8626 | 38° 11' 47.54723" | -120° 00' 49.29476" | 1572.882 |
| DH6395 | 40° 53' 11.57411" | -122° 23' 02.73625" | 306.602 |
| DH6452 | 38° 47' 42.55388" | -120° 08' 52.95313" | 1711.778 |
| DH6458 | 38° 45' 30.92962" | -120° 35' 07.81634" | 1160.160 |
| DH6470 | 39° 19' 22.58210" | -121° 06' 16.06957" | 531.583 |
| DMC_01 | 37° 47' 15.23067" | -119° 00' 09.34243" | 2394.489 |
| EF_SCOTT_01 | 41° 23' 50.57015" | -122° 50' 13.25362" | 847.692 |
| EF_SCOTT_02 | 41° 17' 55.10622" | -122° 43' 28.46381" | 1371.880 |
| EF_SCOTT_03 | 41° 25' 21.80685" | -122° 36' 34.97215" | 1582.430 |
| EF_SCOTT_04 | 41° 25' 39.66915" | -122° 37' 23.90478" | 1560.950 |
| FREDS_FIRE_01 | 38° 47' 25.28661" | -120° 13' 58.52129" | 1852.363 |

| Monument ID | Latitude | Longitude | Ellipsoid (meters) |
|-----------------|-------------------|---------------------|--------------------|
| FREDS_FIRE_02 | 38° 47' 38.64869" | -120° 21' 05.15609" | 1692.38 |
| FREDS_FIRE_03 | 38° 42' 35.89103" | -120° 21' 19.33302" | 1743.400 |
| FREDS_FIRE_04 | 38° 47' 49.17626" | -120° 24' 03.04606" | 1558.480 |
| FREDS_FIRE_05 | 38° 37' 43.91671" | -120° 12' 55.35785" | 2220.970 |
| HR0381 | 37° 44' 25.19648" | -118° 58' 27.68213" | 2257.301 |
| JS4673 | 38° 38' 00.19012" | -120° 10' 36.07660" | 2316.682 |
| KS2043 | 39° 22' 09.50716" | -121° 06' 23.62289" | 612.647 |
| LOW_ELK_1 | 41° 52' 30.94972" | -123° 24' 50.88435" | 429.592 |
| NERC_380 | 38° 30' 09.78626" | -120° 21' 25.73359" | 1399.917 |
| POW_FIRE_01 | 38° 32' 20.02464" | -120° 15' 20.63452" | 1750.381 |
| POW_FIRE_02 | 38° 30' 07.20962" | -120° 19' 17.82206" | 1507.787 |
| POW_FIRE_03 | 38° 28' 32.82500" | -120° 26' 29.15318" | 1118.234 |
| POW_FIRE_04 | 38° 29' 15.15258" | -120° 01' 22.27109" | 2312.898 |
| POW_FIRE_05 | 38° 39' 00.72397" | -120° 07' 50.97779" | 2287.070 |
| ST_EXP_FOREST_1 | 38° 12' 03.59408" | -120° 01' 34.33822" | 1798.269 |
| SUGAR_01 | 41° 19' 18.87933" | -122° 48' 51.57182" | 931.632 |
| VLECK_1 | 38° 56' 59.31459" | -120° 05' 24.71252" | 2036.687 |

To correct the continuously recorded onboard measurements of the aircraft position, QSI concurrently conducted multiple static Global Navigation Satellite System (GNSS) ground surveys (1 Hz recording frequency) over each monument. During post-processing, the static GPS data were triangulated with nearby Continuously Operating Reference Stations (CORS) using the Online Positioning User Service (OPUS¹) for precise positioning. Multiple independent sessions over the same monument were processed to confirm antenna height measurements and to refine position accuracy.

Monuments were established according to the national standard for geodetic control networks, as specified in the Federal Geographic Data Committee (FGDC) Geospatial Positioning Accuracy Standards for geodetic networks.² This standard provides guidelines for classification of monument quality at the 95% confidence interval as a basis for comparing the quality of one control network to another. The monument rating for this project is shown in Table 6.

¹ OPUS is a free service provided by the National Geodetic Survey to process corrected monument positions. <http://www.ngs.noaa.gov/OPUS>.

² Federal Geographic Data Committee, Geospatial Positioning Accuracy Standards (FGDC-STD-007.2-1998). Part 2: Standards for Geodetic Networks, Table 2.1, page 2-3. <http://www.fgdc.gov/standards/projects/FGDC-standards-projects/accuracy/part2/chapter2>

Table 6: Federal Geographic Data Committee monument rating for network accuracy

| Direction | Rating |
|-------------------------------|---------|
| 1.96 * St Dev _{NE} : | 0.020 m |
| 1.96 * St Dev _z : | 0.050 m |

For the USFS Pacific Region 5 LiDAR project, the monument coordinates contributed no more than 5.4 cm of positional error to the geolocation of the final ground survey points and LiDAR, with 95% confidence.

Ground Survey Points (GSPs)

Ground survey points were collected using real time kinematic and post-processed kinematic (PPK), survey techniques. A Trimble R7 base unit was positioned at a nearby monument to broadcast a kinematic correction to a roving Trimble R6 and Trimble R8 GNSS receiver. All GSP measurements were made during periods with a Position Dilution of Precision (PDOP) of ≤ 3.0 with at least six satellites in view of the stationary and roving receivers. When collecting RTK and PPK data, the rover records data while stationary for five seconds, then calculates the pseudo-range position using at least three one-second epochs. Relative errors for any GSP position must be less than 1.5 cm horizontal and 2.0 cm vertical in order to be accepted. See Table 7 for Trimble unit specifications.

GSPs were collected in areas where good satellite visibility was achieved on paved roads and other hard surfaces such as gravel or packed dirt roads. GSP measurements were not taken on highly reflective surfaces such as center line stripes or lane markings on roads due to the increased noise seen in the laser returns over these surfaces. GSPs were collected within as many flightlines as possible; however the distribution of GSPs depended on ground access constraints and monument locations and may not be equitably distributed throughout the study area (Figure 4 and Figure 5).

Table 7: Trimble equipment identification

| Receiver Model | Antenna | OPUS Antenna ID | Use |
|-----------------|--------------------------------------|-----------------|--------|
| Trimble R6 | Integrated GNSS Antenna R6 | TRMR6-3 | Rover |
| Trimble R7 GNSS | Zephyr GNSS Geodetic Model 2 RoHS | TRM57971.00 | Static |
| Trimble R8 | Integrated Antenna R8 Model 2 | TRM_R8_GNSS | Rover |

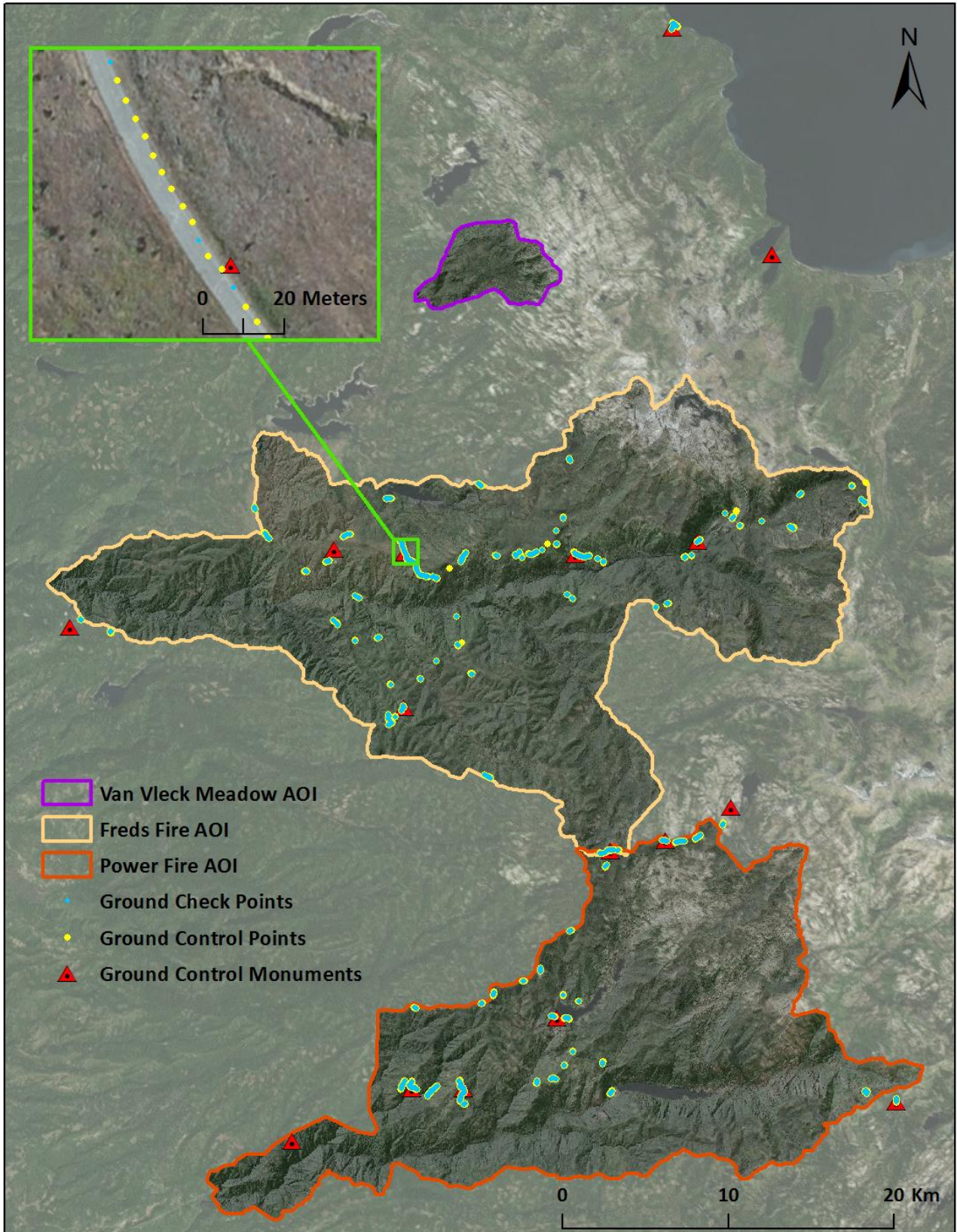


Figure 4: Ground Survey Location Map I

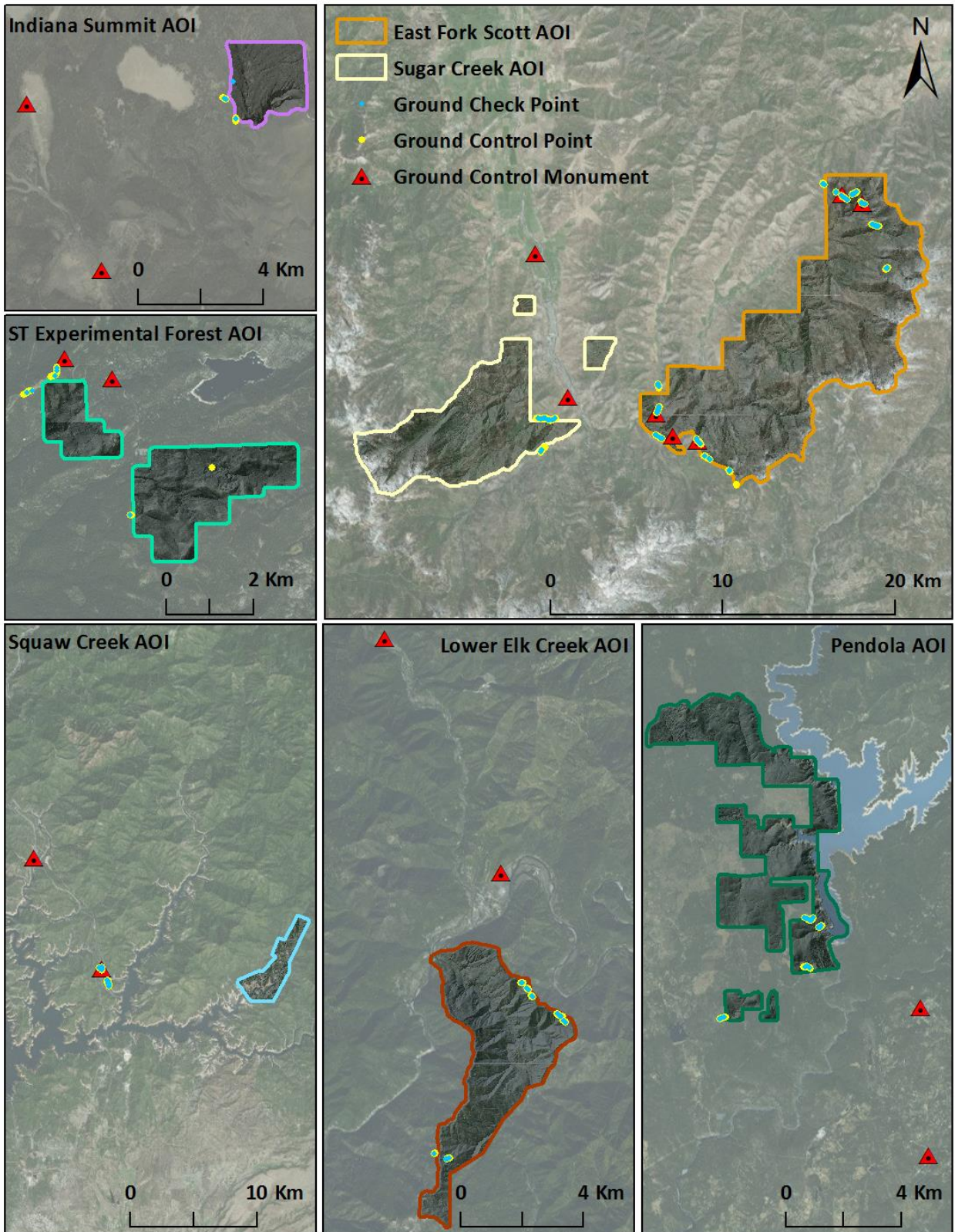


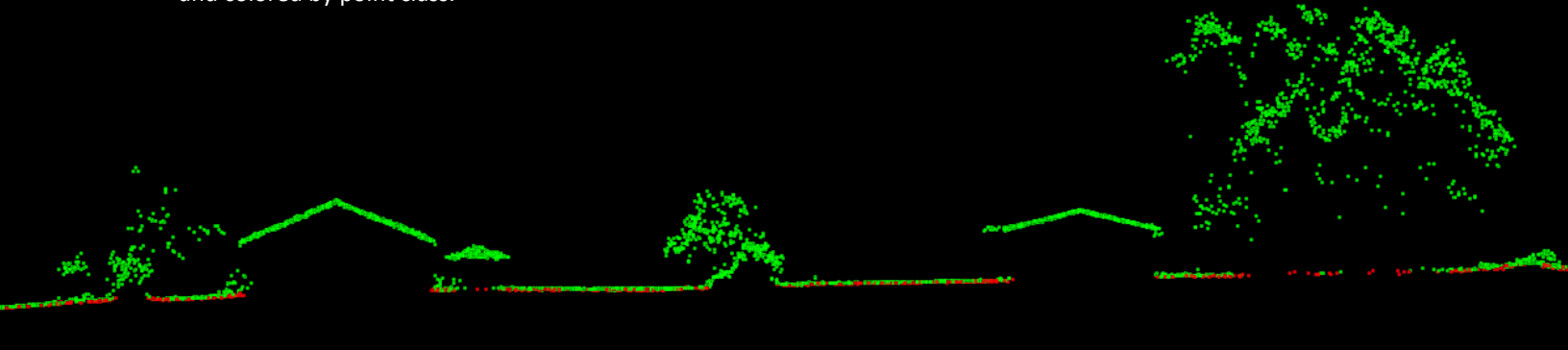


Figure 5: Ground Survey Location Map II

PROCESSING

View of buildings and vegetation in the Lower Elk Creek AOI. The image was created from a 1.5 meter cross-section of the 3D LiDAR point cloud and colored by point class.

Default 
Ground 



LiDAR Data

Upon completion of data acquisition, QSI processing staff initiated a suite of automated and manual techniques to process the data into the requested deliverables. Processing tasks included GPS control computations, smoothed best estimate trajectory (SBET) calculations, kinematic corrections, calculation of laser point position, sensor and data calibration for optimal relative and absolute accuracy, and LiDAR point classification (Table 8). Processing methodologies were tailored for the landscape. Additionally, intensity values were corrected for variability between flightlines per client specifications. Brief descriptions of these tasks are shown in Table 9.

Table 8: ASPRS LAS classification standards applied to the USFS Pacific Region 5 dataset

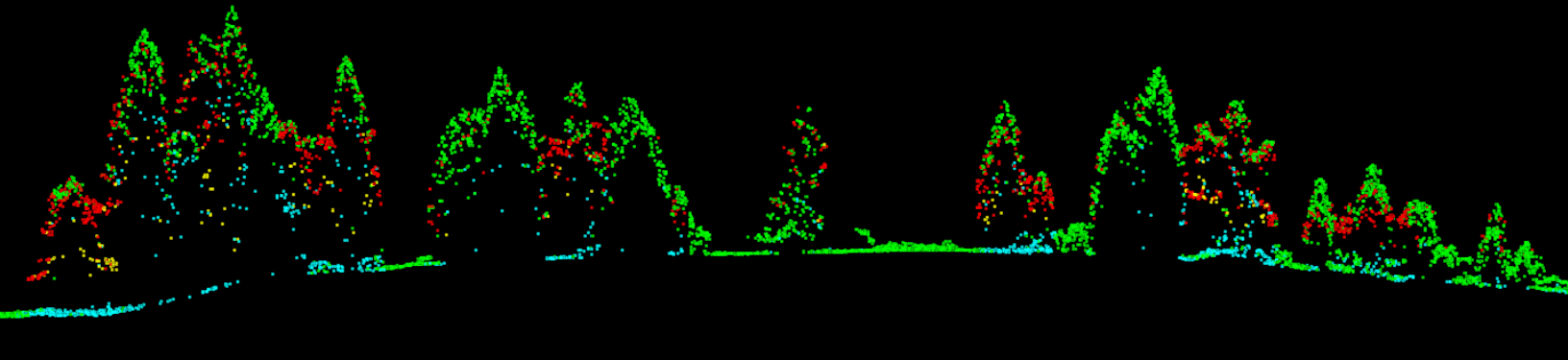
| Classification Number | Classification Name | Classification Description |
|-----------------------|----------------------|---|
| 1 | Default/Unclassified | Laser returns that are not included in the ground class, composed of vegetation and man-made structures |
| 2 | Ground | Laser returns that are determined to be ground using automated and manual cleaning algorithms |
| 7 | Noise | Laser returns that are often associated with birds, scattering from reflective surfaces, or artificial points below the ground surface. |
| 11 | Withheld | Laser returns that have intensity values of 0 or 255 |

Table 9: LiDAR processing workflow

| LiDAR Processing Step | Software Used |
|---|--|
| Resolve kinematic corrections for aircraft position data using kinematic aircraft GPS and static ground GPS data. Develop a smoothed best estimate of trajectory (SBET) file that blends post-processed aircraft position with sensor head position and attitude recorded throughout the survey. | Waypoint Inertial Explorer v.8.5 |
| Calculate laser point position by associating SBET position to each laser point return time, scan angle, intensity, etc. Create raw laser point cloud data for the entire survey in *.las (ASPRS v. 1.2) format. Convert data to orthometric elevations by applying a geoid03 correction. | Waypoint Inertial Explorer v.8.5 Leica Cloudpro v. 1.2.1 |
| Import raw laser points into manageable blocks (less than 500 MB) to perform manual relative accuracy calibration and filter erroneous points. Classify ground points for individual flight lines. | TerraScan v.15 |
| Using ground classified points per each flight line, test the relative accuracy. Perform automated line-to-line calibrations for system attitude parameters (pitch, roll, heading), mirror flex (scale) and GPS/IMU drift. Calculate calibrations on ground classified points from paired flight lines and apply results to all points in a flight line. Use every flight line for relative accuracy calibration. | TerraMatch v.15 |
| Classify resulting data to ground and other client designated ASPRS classifications (Table 8). Assess statistical absolute accuracy via direct comparisons of ground classified points to ground control survey data. | Las Monkey (QSI proprietary) v.2.0 TerraScan v.15 TerraModeler v.15 |
| Generate bare earth models as triangulated surfaces. Generate highest hit models as a surface expression of all classified points. Export all surface models as a ENVI (.dat) file format at a 1 meter pixel resolution. | TerraScan v.15 TerraModeler v.15 ArcMap v. 10.1 |
| Correct intensity values for variability and export intensity images as an ENVI (.dat) file format at a 0.5 meter pixel resolution. | Las Monkey (QSI proprietary) v.2.0 LAS DZ Ortho Creator (QSI proprietary) ArcMap v. 10.1 |

This image shows a 1-meter cross-section of a vegetated slope from the Lower Elk Creek AOI. The 3D LiDAR point cloud is colored by echo.

Only Echo █
First of Many █
Intermediate █
Last of Many █



LiDAR Density

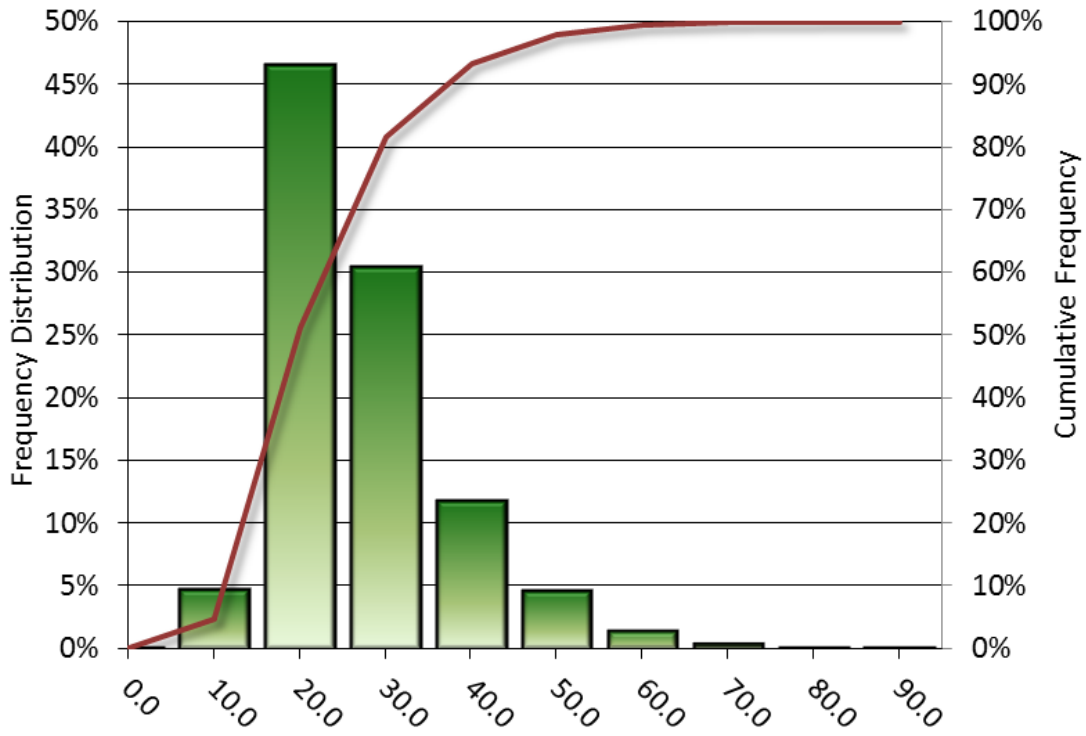
The acquisition parameters were designed to acquire an average first-return density of 8 points/m². First return density describes the density of pulses emitted from the laser that return at least one echo to the system. Multiple returns from a single pulse were not considered in first return density analysis. Some types of surfaces (e.g., breaks in terrain, water and steep slopes) may have returned fewer pulses than originally emitted by the laser. First returns typically reflect off the highest feature on the landscape within the footprint of the pulse. In forested or urban areas the highest feature could be a tree, building or power line, while in areas of unobstructed ground, the first return will be the only echo and represents the bare earth surface.

The density of ground-classified LiDAR returns was also analyzed for this project. Terrain character, land cover, and ground surface reflectivity all influenced the density of ground surface returns. In vegetated areas, fewer pulses may penetrate the canopy, resulting in lower ground density.

The cumulative average first-return density of LiDAR data for the USFS Pacific Region 5 project was 22.05 points/m² while the cumulative average ground classified density was 2.61 points/m² (Table 10). The statistical and spatial distributions of cumulative first return densities and cumulative ground-classified return densities per 100m x 100m cell are portrayed in Figure 6 through Figure 11. Individual frequency histograms displaying density analysis by AOI can be seen in Appendix B.

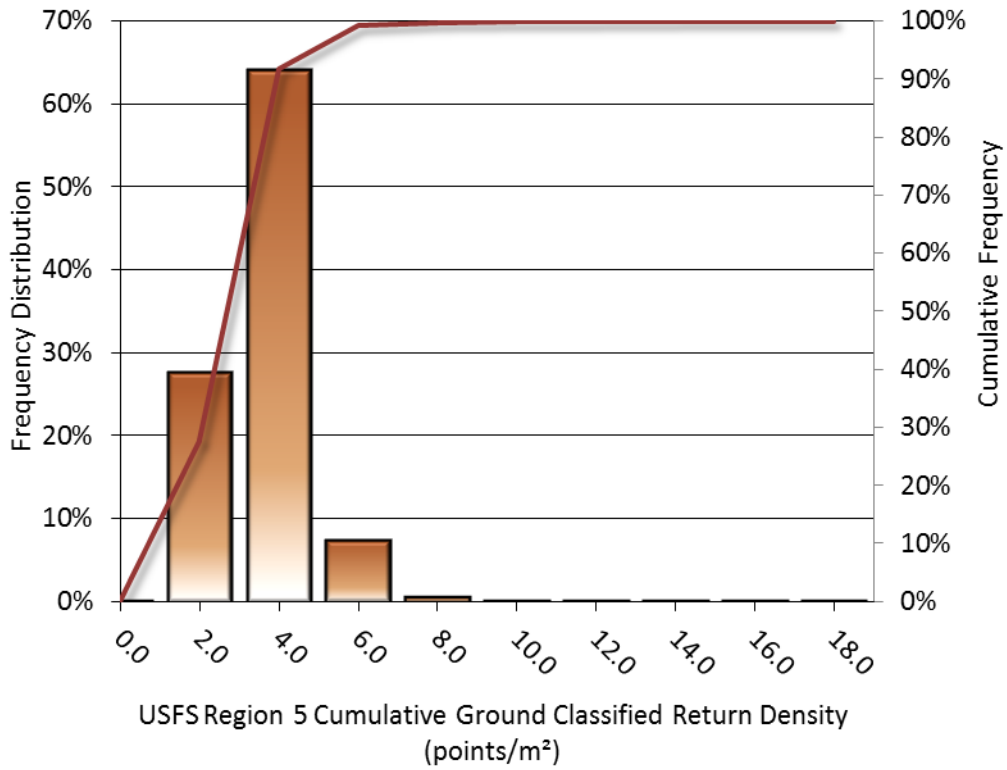
Table 10: Average LiDAR point densities

| Area of Interest | First Return Point Density | Ground Classified Point Density |
|------------------------|-----------------------------|---------------------------------|
| Indiana Summit RNA | 13.26 points/m ² | 2.65 points/m ² |
| East Fork Scotts River | 14.42 points/m ² | 2.67 points/m ² |
| Lower Elk Creek | 17.73 points/m ² | 1.78 points/m ² |
| Pendola | 11.00 points/m ² | 1.09 points/m ² |
| Squaw Creek | 10.50 points/m ² | 2.02 points/m ² |
| ST Experimental Forest | 11.85 points/m ² | 1.91 points/m ² |
| Sugar Creek | 16.11 points/m ² | 2.36 points/m ² |
| Van Vleck Meadows | 10.86 points/m ² | 2.02 points/m ² |
| Freds Fire | 24.92 points/m ² | 2.73 points/m ² |
| Power Fire | 23.27 points/m ² | 2.65 points/m ² |
| Cumulative | 22.05 points/m ² | 2.61 points/m ² |



USFS Region 5 Cumulative First Return Point Density (points/m²)

Figure 6: Frequency distribution of first return densities per 100 x 100 m cell



USFS Region 5 Cumulative Ground Classified Return Density (points/m²)

Figure 7: Frequency distribution of ground return densities per 100 x 100 m cell

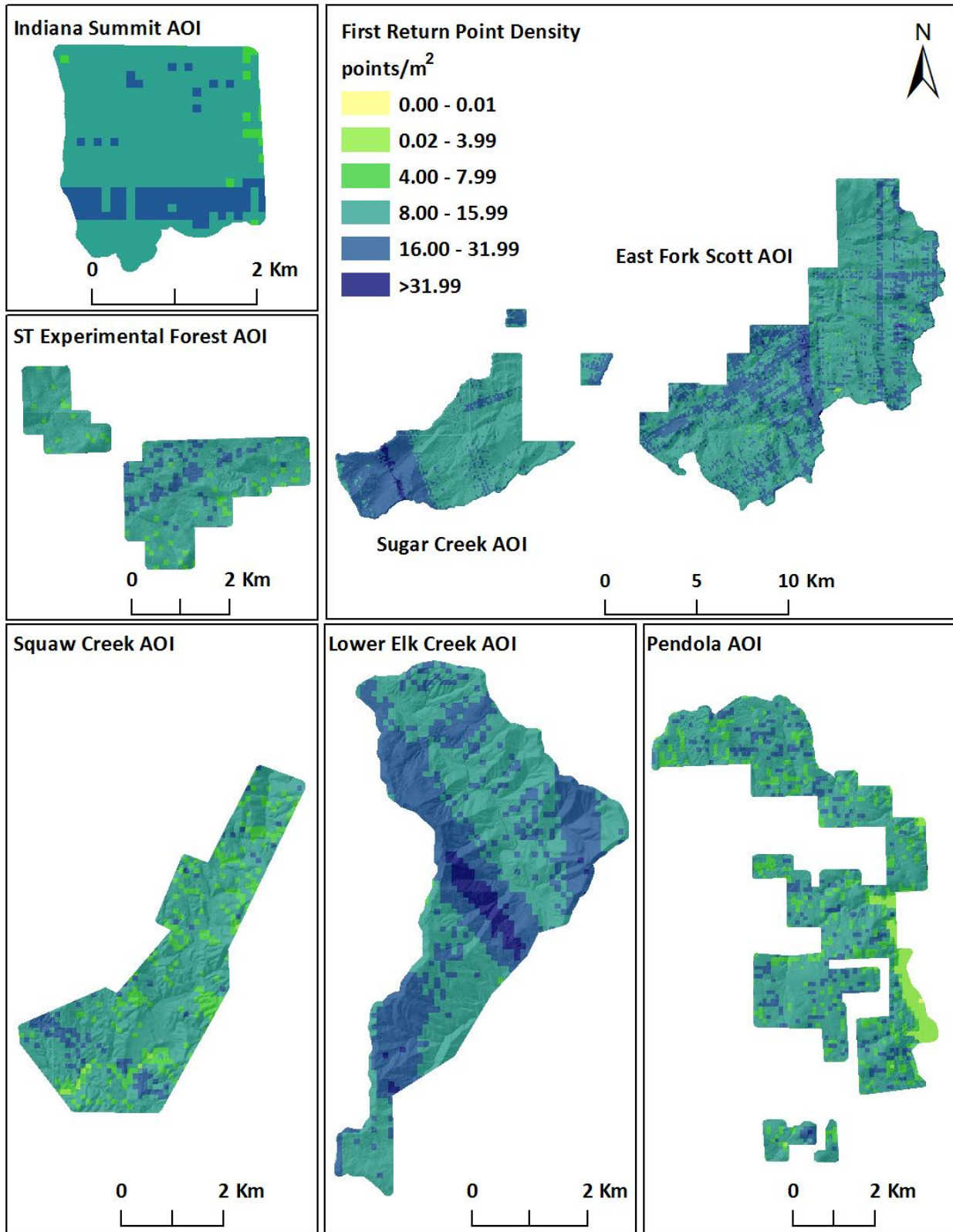


Figure 8: One of two first return density maps of the USFS Pacific Region 5 sites (100 m x 100 m cells)

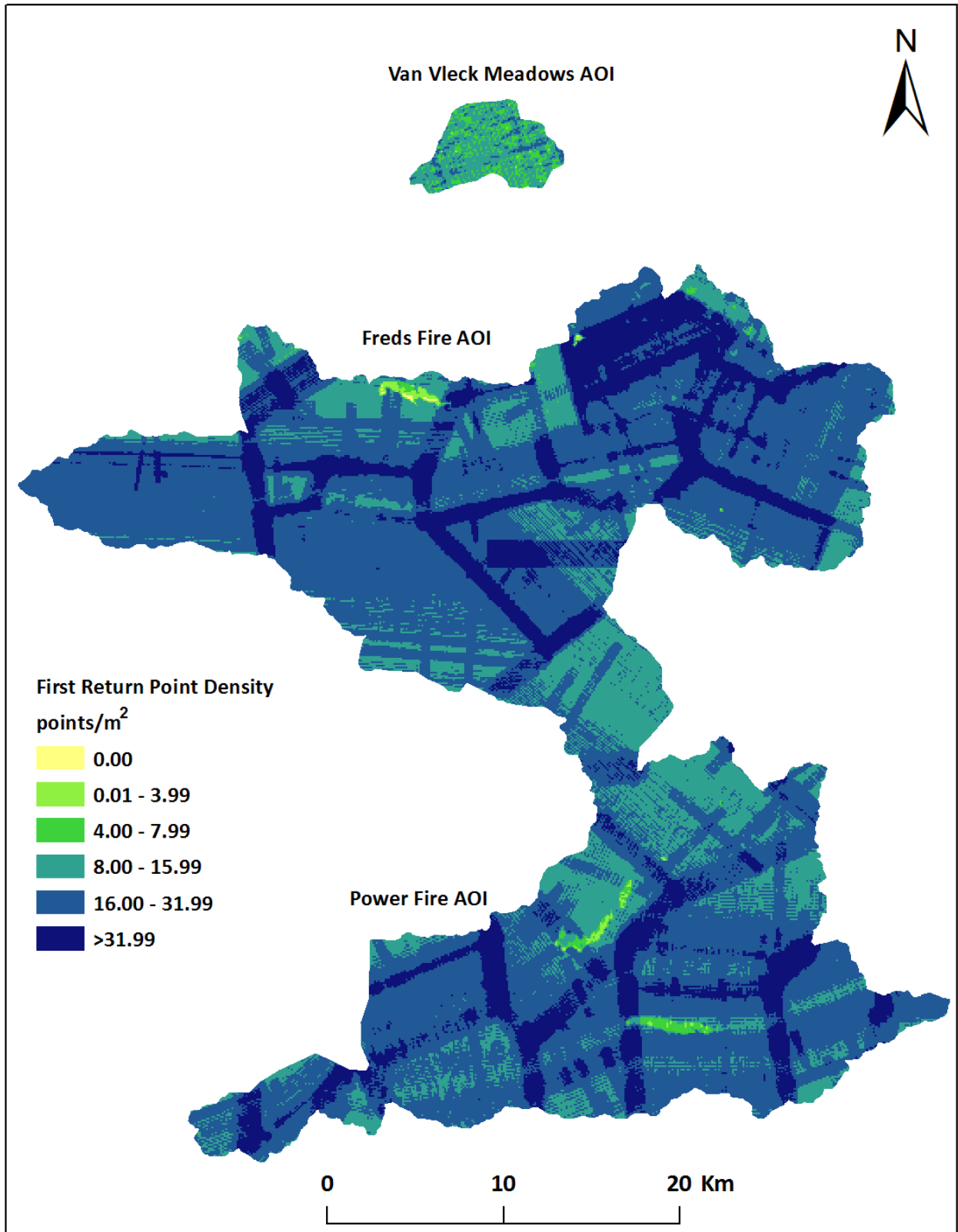


Figure 9: Two of two first return density maps of the USFS Pacific Region 5 sites (100 m x 100 m cells)

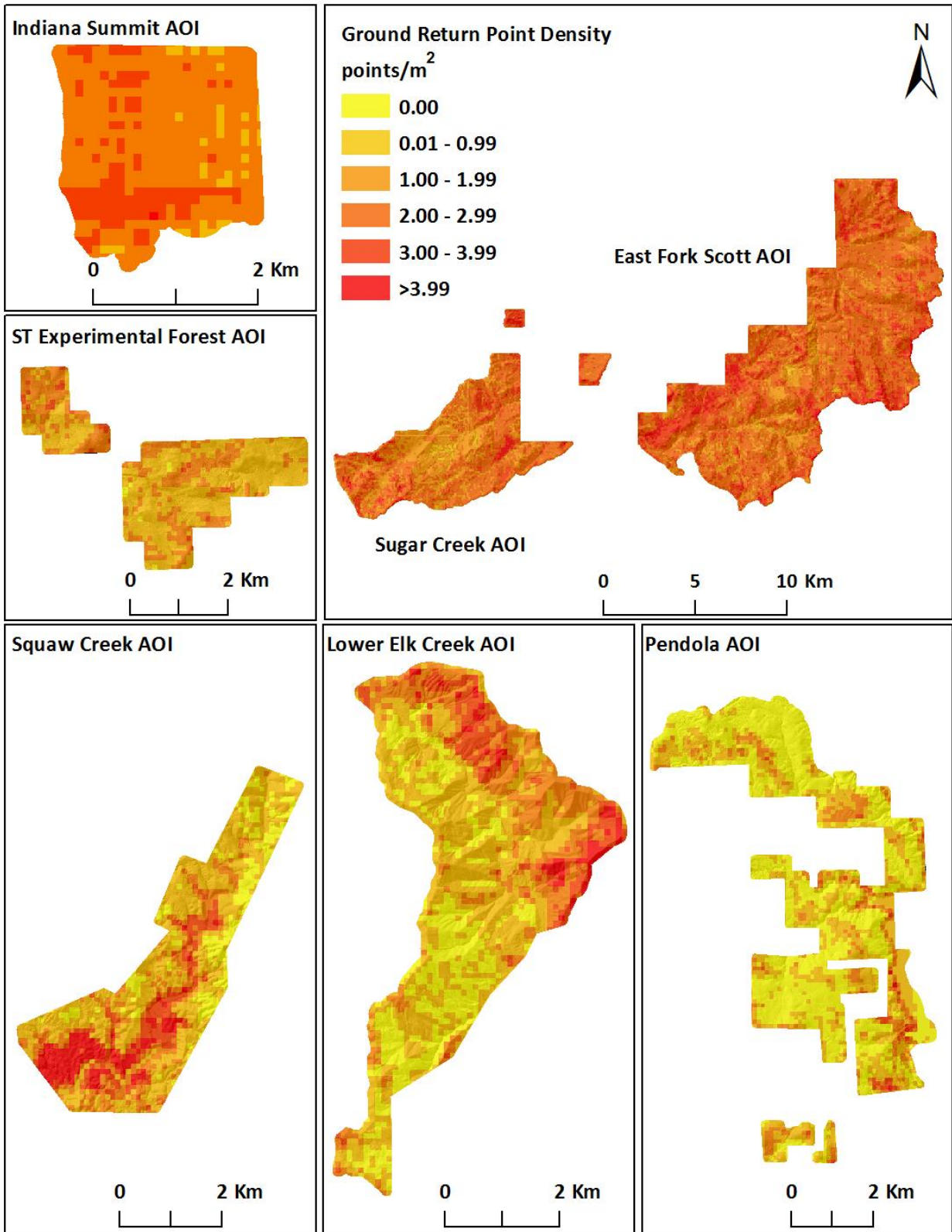


Figure 10: One of two ground density maps of the USFS Pacific Region 5 site (100 m x 100 m cells)

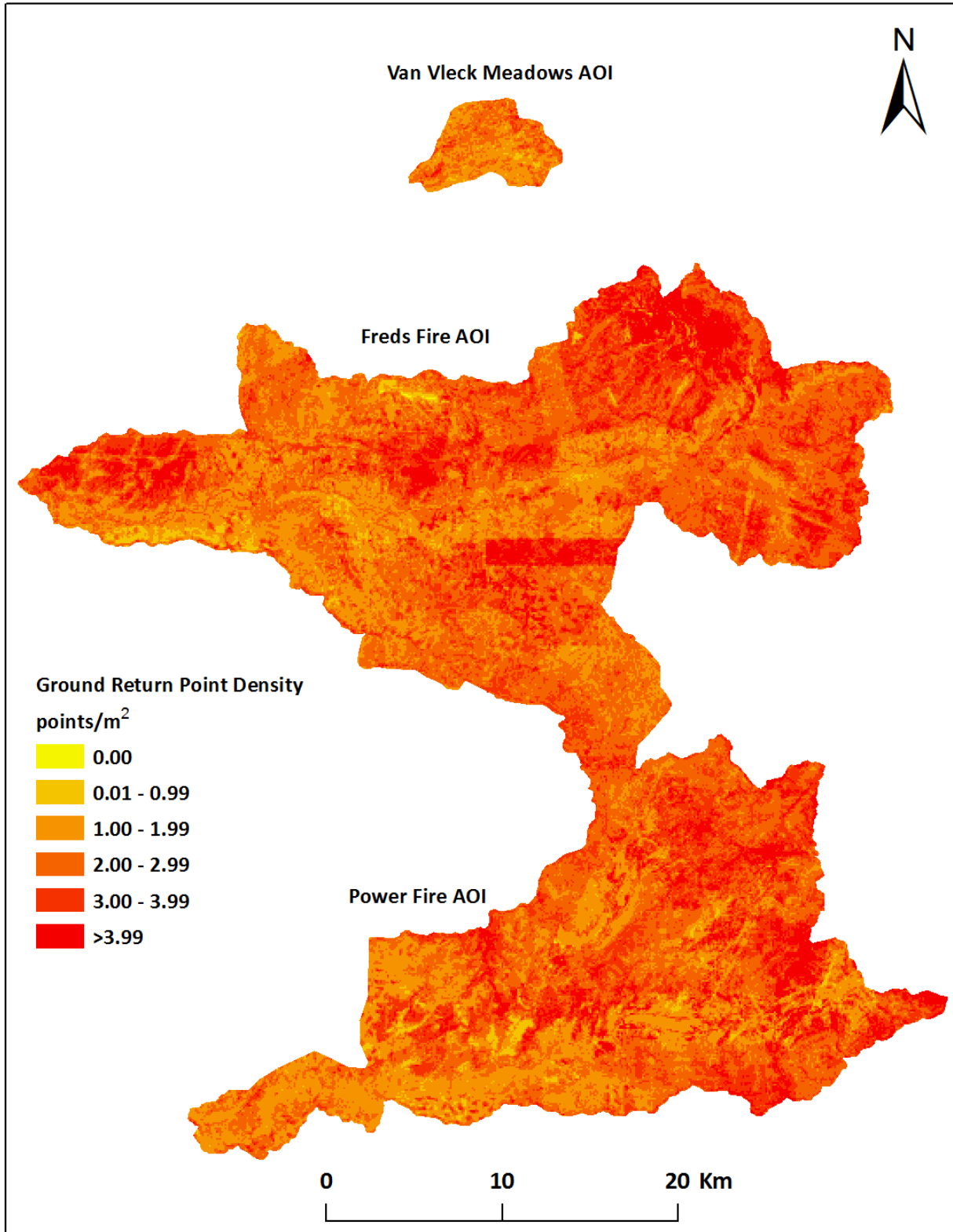


Figure 11: Two of two ground density maps of the USFS Pacific Region 5 site (100 m x 100 m cells)

LiDAR Accuracy Assessments

The accuracy of the LiDAR data collection can be described in terms of absolute accuracy (the consistency of the data with external data sources) and relative accuracy (the consistency of the dataset with itself). See Appendix A for further information on sources of error and operational measures used to improve relative accuracy.

LiDAR Absolute Accuracy

Absolute accuracy was assessed using Fundamental Vertical Accuracy (FVA) reporting designed to meet guidelines presented in the FGDC National Standard for Spatial Data Accuracy³. FVA compares known RTK ground check point data collected on open, bare earth surfaces with level slope (<20°) to the triangulated surface generated by the LiDAR points. FVA is a measure of the accuracy of LiDAR point data in open areas where the LiDAR system has a high probability of measuring the ground surface and is evaluated at the 95% confidence interval ($1.96 * RMSE$), as shown in Table 11. The mean and standard deviation (σ) of divergence between the ground surface model and the ground survey point coordinates are also considered during accuracy assessment. These statistics assume the error for x, y and z is normally distributed, and therefore the skew and kurtosis of the distribution is also evaluated. For the USFS Pacific Region 5 survey, 618 ground check points were collected in total resulting in a FVA of 0.057 meters (Figure 12).

QSI also assessed accuracy using ground control point data. Although these points were used in the calibration and post-processing of the LiDAR point cloud, they still provide a good indication of the overall accuracy of the LiDAR dataset, and have been provided in Table 9. For the USFS Pacific Region 5 survey, 5538 ground control points were collected in total resulting in an absolute accuracy of 0.056 meters (Figure 13). Absolute accuracies for individual AOIs can be viewed in Appendix C.

³ Federal Geographic Data Committee, Geospatial Positioning Accuracy Standards (FGDC-STD-007.3-1998). Part 3: National Standard for Spatial Data Accuracy. <http://www.fgdc.gov/standards/projects/FGDC-standards-projects/accuracy/part3/chapter3>

Table 11: Fundamental Vertical Accuracy

| Fundamental Vertical Accuracy | | | | | | | | | | | |
|-------------------------------|----------------|------------------------|-----------------|---------|-------------|------------------------|-------------|-------------------|------------|------------|------------|
| | Indiana Summit | East Fork Scotts River | Lower Elk Creek | Pendola | Squaw Creek | ST Experimental Forest | Sugar Creek | Van Vleck Meadows | Freds Fire | Power Fire | Cumulative |
| Sample Size | 4 | 71 | 18 | 19 | 23 | 6 | 11 | 13 | 274 | 179 | 618 |
| FVA (1.96* RMSE) | -0.025 m | 0.051 m | 0.068 m | 0.053 m | 0.043 m | 0.040 m | 0.046 m | 0.096 m | 0.055 m | 0.059 m | 0.057 m |
| Average | -0.025 m | 0.005 m | -0.01 m | 0.003 m | -0.003 m | -0.002 m | -0.009 m | -0.007 m | 0.002 m | -0.002 m | 0.000 m |
| Median | -0.034 m | 0.007 m | -0.012 m | 0.000 m | -0.004 m | -0.004 m | -0.010 m | -0.021 m | 0.005 m | -0.001 m | 0.00 m |
| RMSE | 0.044 m | 0.026 m | 0.035 m | 0.027 m | 0.022 m | 0.021 m | 0.024 m | 0.049 m | 0.028 m | 0.030 m | 0.029 m |
| Standard Deviation (1σ) | 0.042 m | 0.026 m | 0.034 m | 0.028 m | 0.022 m | 0.022 m | 0.023 m | 0.051 m | 0.028 m | 0.030 m | 0.029 m |

Table 12: Absolute Accuracy of Ground Control Points

| Absolute Accuracy | | | | | | | | | | | |
|-------------------------|----------------|------------------------|-----------------|---------|-------------|------------------------|-------------|-------------------|------------|------------|------------|
| | Indiana Summit | East Fork Scotts River | Lower Elk Creek | Pendola | Squaw Creek | ST Experimental Forest | Sugar Creek | Van Vleck Meadows | Freds Fire | Power Fire | Cumulative |
| Sample Size | 34 | 630 | 167 | 170 | 23 | 210 | 52 | 109 | 2465 | 1599 | 5538 |
| 1.96*RMSE | 0.075 m | 0.052 m | 0.058 m | 0.052 m | 0.043 m | 0.045 m | 0.047 m | 0.079 m | 0.057 m | 0.056 m | 0.056 m |
| Average | -0.005 m | 0.001 m | -0.005 m | 0.001 m | -0.003 m | -0.004 m | -0.004 m | -0.004 m | 0.001 m | -0.002 m | 0.000 m |
| Median | -0.002 m | 0.002 m | -0.003 m | 0.002 m | -0.004 m | -0.005 m | -0.001 m | -0.016 m | 0.004 m | -0.002 m | 0.001 m |
| RMSE | 0.038 m | 0.027 m | 0.029 m | 0.026 m | 0.022 m | 0.023 m | 0.024 m | 0.041 m | 0.029 m | 0.029 m | 0.029 m |
| Standard Deviation (1σ) | 0.038 m | 0.027 m | 0.029 m | 0.026 m | 0.022 m | 0.023 m | 0.024 m | 0.041 m | 0.029 m | 0.029 m | 0.029 m |

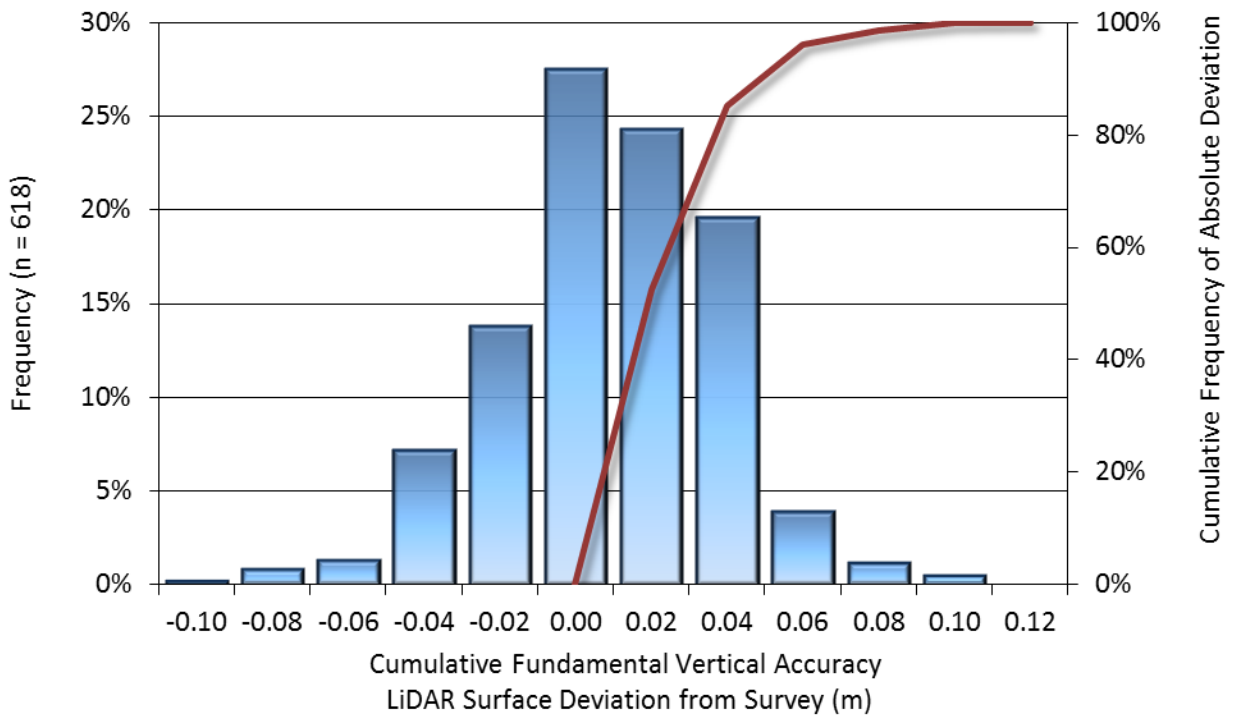


Figure 12: Cumulative frequency histogram for LiDAR surface deviation from the USGS Region 5 ground check point values

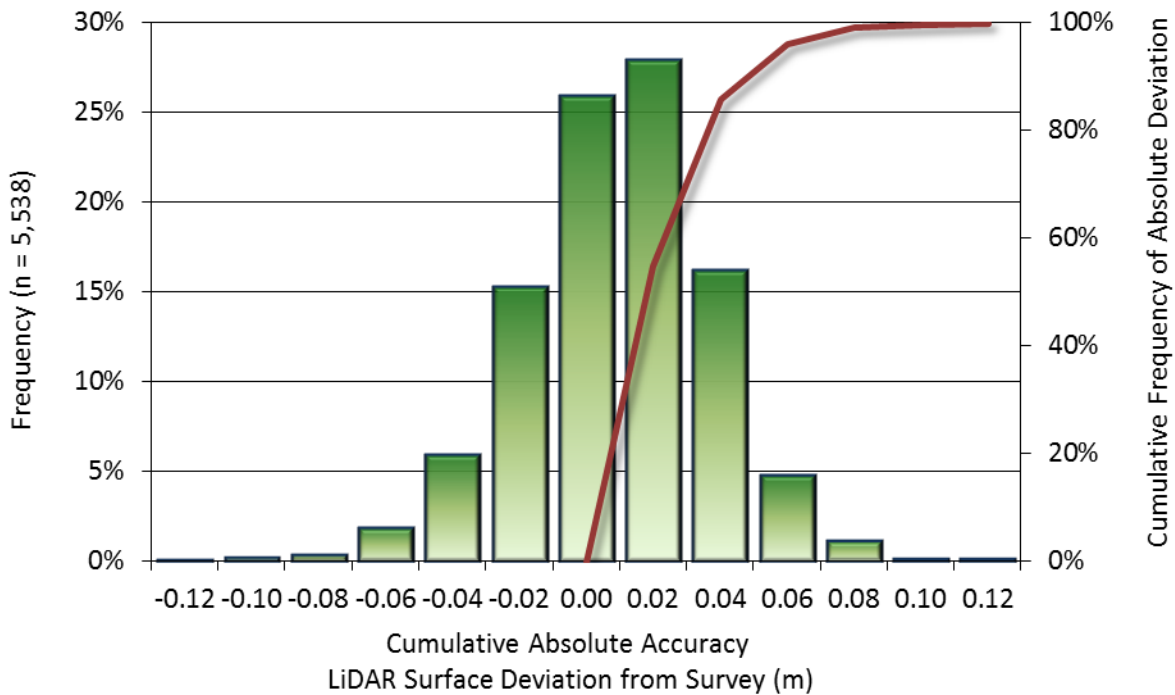


Figure 13: Cumulative frequency histogram for LiDAR surface deviation from the USGS Region 5 ground control point value

LiDAR Vertical Relative Accuracy

Relative vertical accuracy refers to the internal consistency of the data set as a whole: the ability to place an object in the same location given multiple flight lines, GPS conditions, and aircraft attitudes. When the LiDAR system is well calibrated, the swath-to-swath vertical divergence is low (<0.10 meters). The relative vertical accuracy was computed by comparing the ground surface model of each individual flight line with its neighbors in overlapping regions. The average (mean) line to line relative vertical accuracy for the USFS Pacific Region 5 LiDAR project was 0.046 meters (Figure 14, Table 13) Vertical Relative accuracies for individual AOIs can be viewed in Appendix D.

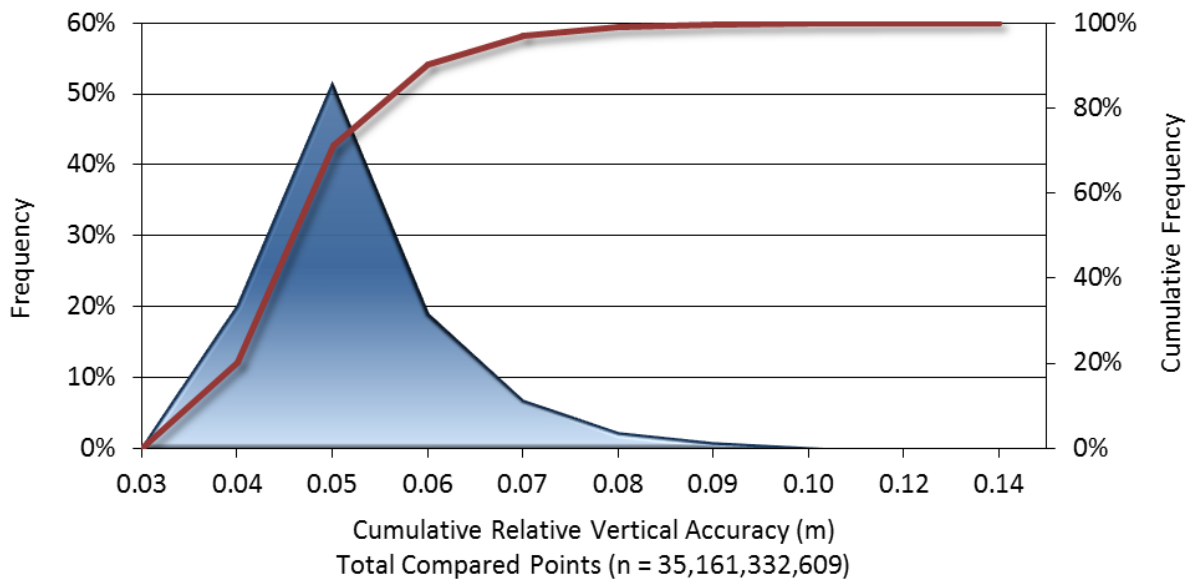


Figure 14: Cumulative frequency plot for the relative vertical accuracy between flight lines in the USFS Region 5 Project Area

Table 13: Vertical Relative Accuracy

| Vertical Relative Accuracy | | | | | | | | | | | |
|----------------------------|----------------|------------------------|-----------------|---------|-------------|------------------------|-------------|-------------------|------------|------------|------------|
| | Indiana Summit | East Fork Scotts River | Lower Elk Creek | Pendola | Squaw Creek | ST Experimental Forest | Sugar Creek | Van Vleck Meadows | Freds Fire | Power Fire | Cumulative |
| Surfaces | 24 | 166 | 72 | 46 | 26 | 45 | 144 | 66 | 800 | 563 | 1952 |
| Average | 0.049 m | 0.040 m | 0.053 m | 0.042 m | 0.037 m | 0.038 m | 0.050 m | 0.043 m | 0.046 m | 0.048 m | 0.046 m |
| Median | 0.045 m | 0.041 m | 0.057 m | 0.042 m | 0.037 m | 0.038 m | 0.050 m | 0.037 m | 0.045 m | 0.047 m | 0.045 m |
| RMSE | 0.053 m | 0.042 m | 0.059 m | 0.044 m | 0.039 m | 0.038 m | 0.053 m | 0.042 m | 0.047 m | 0.050 m | 0.048 m |
| Standard Deviation (1σ) | 0.016 m | 0.005 m | 0.011 m | 0.006 m | 0.006 m | 0.003 m | 0.012 m | 0.009 m | 0.008 m | 0.010 m | 0.010 m |

CERTIFICATIONS

I, Christopher Glantz, being duly registered as a Professional Land Surveyor in and by the state of California, hereby certify that the methodologies, static GNSS occupations used during airborne flights, and ground survey point collection were performed using commonly accepted Standard Practices. Field work conducted for this report was conducted between October 6, 2014 and June 5, 2015.

Accuracy statistics shown in the Accuracy Section of this Report have been reviewed by me and found to meet the "National Standard for Spatial Data Accuracy".



10/1/2015

Christopher Glantz, PLS
Professional Land Surveyor
Quantum Spatial, Inc.
Corvallis, OR 97333



SELECTED IMAGES



Figure 15: View looking east over the Freds Fire AOI. This image was created from the gridded bare earth model colored by elevation, and overlaid with the above-ground LiDAR point cloud

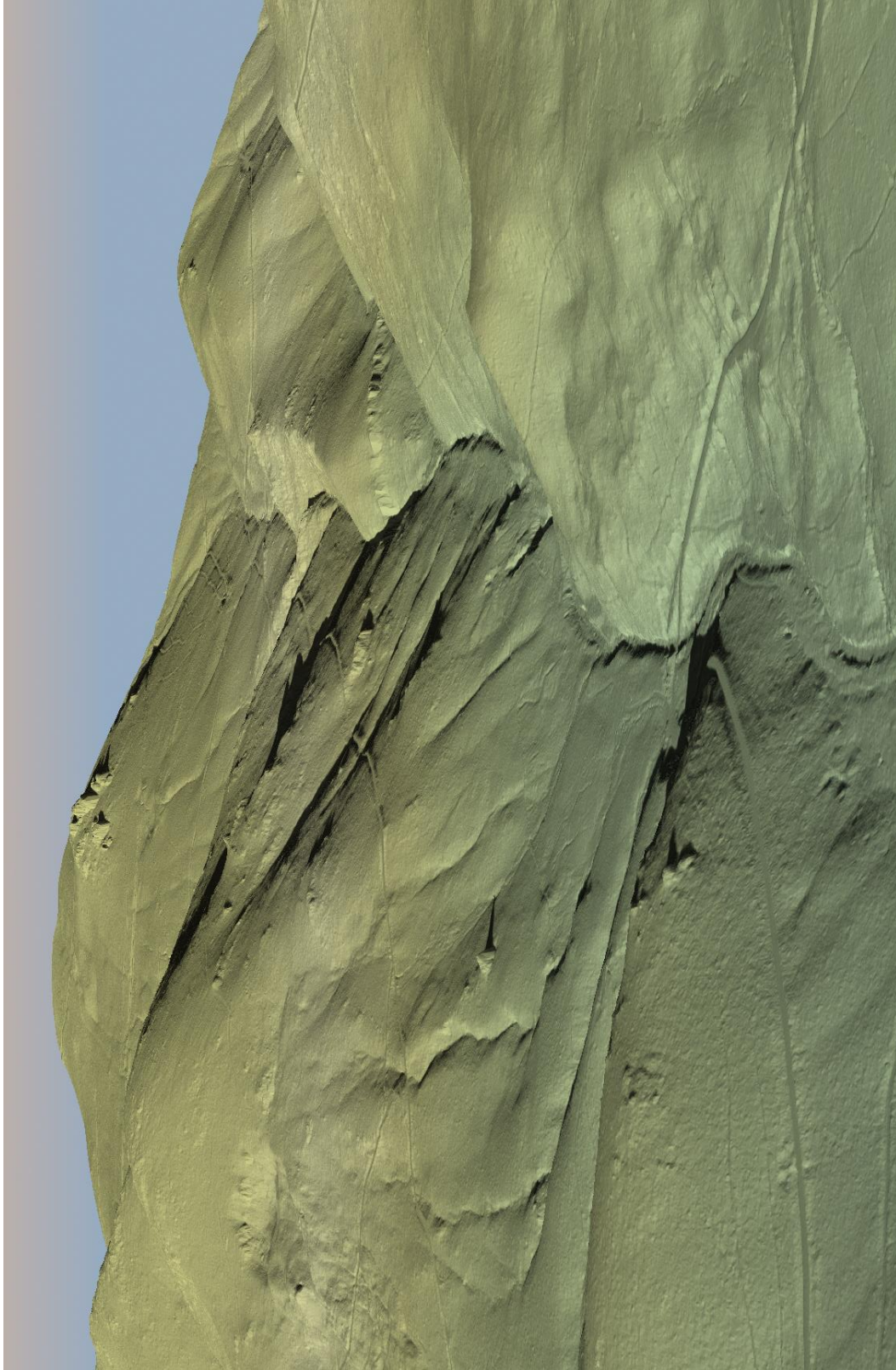


Figure 16: This image displays the view looking northeast across the East Fork Scott River AOI. The image was created from the bare earth model colored by elevation.

1-sigma (σ) Absolute Deviation: Value for which the data are within one standard deviation (approximately 68th percentile) of a normally distributed data set.

1.96 * RMSE Absolute Deviation: Value for which the data are within two standard deviations (approximately 95th percentile) of a normally distributed data set, based on the FGDC standards for Fundamental Vertical Accuracy (FVA) reporting.

Accuracy: The statistical comparison between known (surveyed) points and laser points. Typically measured as the standard deviation (σ) and root mean square error (RMSE).

Absolute Accuracy: The vertical accuracy of LiDAR data is described as the mean and standard deviation (σ) of divergence of LiDAR point coordinates from ground survey point coordinates. To provide a sense of the model predictive power of the dataset, the root mean square error (RMSE) for vertical accuracy is also provided. These statistics assume the error distributions for x, y and z are normally distributed, and thus we also consider the skew and kurtosis of distributions when evaluating error statistics.

Relative Accuracy: Relative accuracy refers to the internal consistency of the data set; i.e., the ability to place a laser point in the same location over multiple flight lines, GPS conditions and aircraft attitudes. Affected by system attitude offsets, scale and GPS/IMU drift, internal consistency is measured as the divergence between points from different flight lines within an overlapping area. Divergence is most apparent when flight lines are opposing. When the LiDAR system is well calibrated, the line-to-line divergence is low (<10 cm).

Root Mean Square Error (RMSE): A statistic used to approximate the difference between real-world points and the LiDAR points. It is calculated by squaring all the values, then taking the average of the squares and taking the square root of the average.

Data Density: A common measure of LiDAR resolution, measured as points per square meter.

Digital Elevation Model (DEM): File or database made from surveyed points, containing elevation points over a contiguous area. Digital terrain models (DTM) and digital surface models (DSM) are types of DEMs. DTMs consist solely of the bare earth surface (ground points), while DSMs include information about all surfaces, including vegetation and man-made structures.

Intensity Values: The peak power ratio of the laser return to the emitted laser, calculated as a function of surface reflectivity.

Nadir: A single point or locus of points on the surface of the earth directly below a sensor as it progresses along its flight line.

Overlap: The area shared between flight lines, typically measured in percent. 100% overlap is essential to ensure complete coverage and reduce laser shadows.

Pulse Rate (PR): The rate at which laser pulses are emitted from the sensor; typically measured in thousands of pulses per second (kHz).

Pulse Returns: For every laser pulse emitted, the number of wave forms (i.e., echos) reflected back to the sensor. Portions of the wave form that return first are the highest element in multi-tiered surfaces such as vegetation. Portions of the wave form that return last are the lowest element in multi-tiered surfaces.

Real-Time Kinematic (RTK) Survey: A type of surveying conducted with a GPS base station deployed over a known monument with a radio connection to a GPS rover. Both the base station and rover receive differential GPS data and the baseline correction is solved between the two. This type of ground survey is accurate to 1.5 cm or less.

Post-Processed Kinematic (PPK) Survey: GPS surveying is conducted with a GPS rover collecting concurrently with a GPS base station set up over a known monument. Differential corrections and precisions for the GNSS baselines are computed and applied after the fact during processing. This type of ground survey is accurate to 1.5 cm or less.

Scan Angle: The angle from nadir to the edge of the scan, measured in degrees. Laser point accuracy typically decreases as scan angles increase.

Native LiDAR Density: The number of pulses emitted by the LiDAR system, commonly expressed as pulses per square meter.

APPENDIX A: ACCURACY CONTROLS

Relative Accuracy Calibration Methodology:

Manual System Calibration: Calibration procedures for each mission require solving geometric relationships that relate measured swath-to-swath deviations to misalignments of system attitude parameters. Corrected scale, pitch, roll and heading offsets were calculated and applied to resolve misalignments. The raw divergence between lines was computed after the manual calibration was completed and reported for each survey area.

Automated Attitude Calibration: All data were tested and calibrated using TerraMatch automated sampling routines. Ground points were classified for each individual flight line and used for line-to-line testing. System misalignment offsets (pitch, roll and heading) and scale were solved for each individual mission and applied to respective mission datasets. The data from each mission were then blended when imported together to form the entire area of interest.

Automated Z Calibration: Ground points per line were used to calculate the vertical divergence between lines caused by vertical GPS drift. Automated Z calibration was the final step employed for relative accuracy calibration.

LiDAR accuracy error sources and solutions:

| Type of Error | Source | Post Processing Solution |
|-----------------------------------|------------------------------|---|
| GPS (Static/Kinematic) | Long Base Lines | None |
| | Poor Satellite Constellation | None |
| | Poor Antenna Visibility | Reduce Visibility Mask |
| Relative Accuracy | Poor System Calibration | Recalibrate IMU and sensor offsets/settings |
| | Inaccurate System | None |
| Laser Noise | Poor Laser Timing | None |
| | Poor Laser Reception | None |
| | Poor Laser Power | None |
| | Irregular Laser Shape | None |

Operational measures taken to improve relative accuracy:

Low Flight Altitude: Terrain following was employed to maintain a constant above ground level (AGL). Laser horizontal errors are a function of flight altitude above ground (about 1/3000th AGL flight altitude).

Focus Laser Power at narrow beam footprint: A laser return must be received by the system above a power threshold to accurately record a measurement. The strength of the laser return (i.e., intensity) is a function of laser emission power, laser footprint, flight altitude and the reflectivity of the target. While surface reflectivity cannot be controlled, laser power can be increased and low flight altitudes can be maintained.

Reduced Scan Angle: Edge-of-scan data can become inaccurate. The scan angle was reduced to a maximum of $\pm 15^\circ$ from nadir, creating a narrow swath width and greatly reducing laser shadows from trees and buildings.

Quality GPS: Flights took place during optimal GPS conditions (e.g., 6 or more satellites and PDOP [Position Dilution of Precision] less than 3.0). Before each flight, the PDOP was determined for the survey day. During all flight times, a dual frequency DGPS base station recording at 1 second epochs was utilized and a maximum baseline length between the aircraft and the control points was less than 13 nm at all times.

Ground Survey: Ground survey point accuracy (<1.5 cm RMSE) occurs during optimal PDOP ranges and targets a minimal baseline distance of 4 miles between GPS rover and base. Robust statistics are, in part, a function of sample size (n) and distribution. Ground survey points are distributed to the extent possible throughout multiple flight lines and across the survey area.

50% Side-Lap (100% Overlap): Overlapping areas are optimized for relative accuracy testing. Laser shadowing is minimized to help increase target acquisition from multiple scan angles. Ideally, with a 50% side-lap, the nadir portion of one flight line coincides with the swath edge portion of overlapping flight lines. A minimum of 50% side-lap with terrain-followed acquisition prevents data gaps.

Opposing Flight Lines: All overlapping flight lines have opposing directions. Pitch, roll and heading errors are amplified by a factor of two relative to the adjacent flight line(s), making misalignments easier to detect and resolve.

APPENDIX B: DENSITY RESULTS

Indiana Summit AOI:

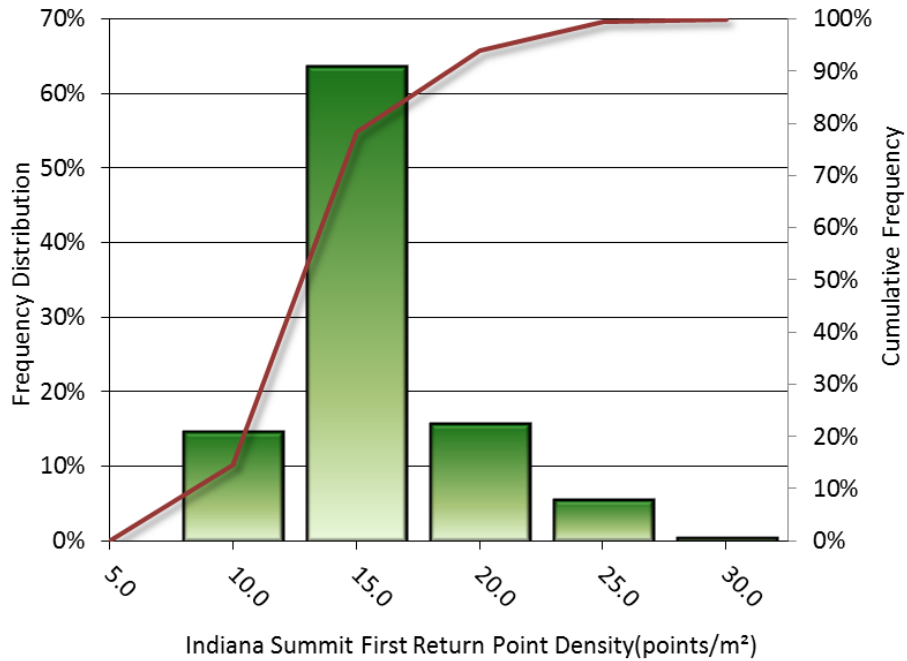


Figure 18: Frequency distribution of first return densities per 100 m x 100 m cell

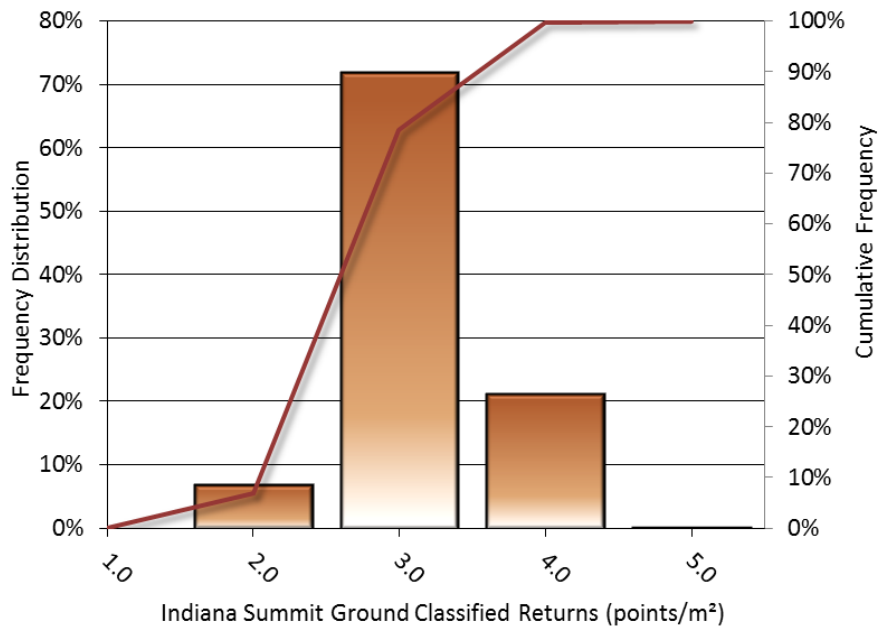


Figure 19: Frequency distribution of ground return densities per 100 m x 100 m cell

East Forks Scott AOI:

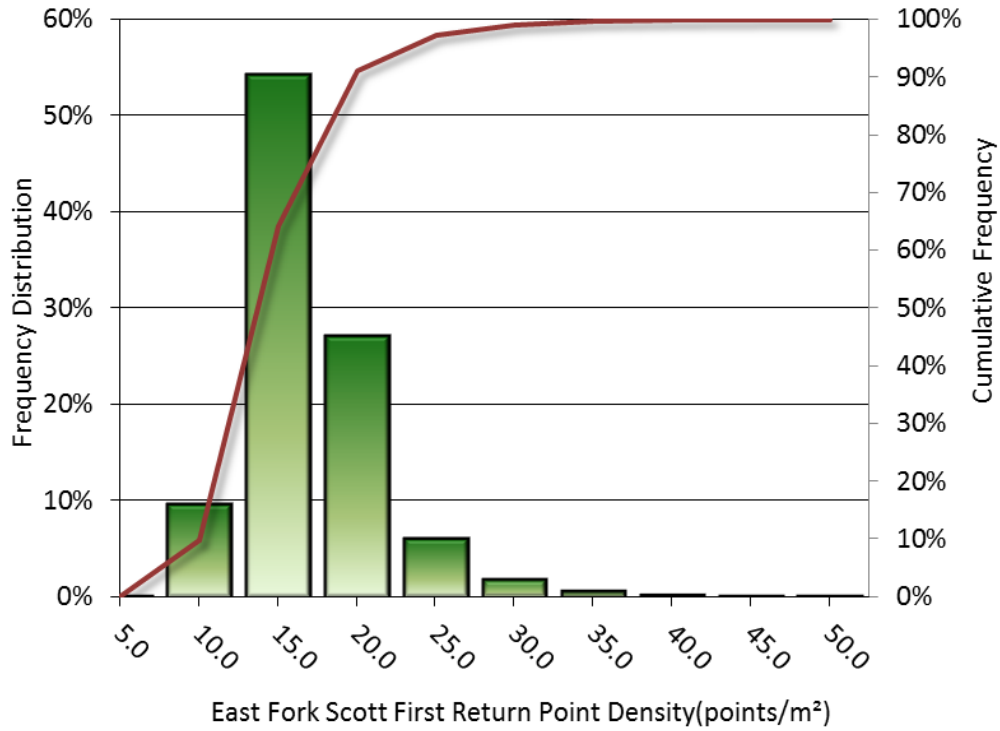


Figure 20: Frequency distribution of first return densities per 100 m x 100 m cell

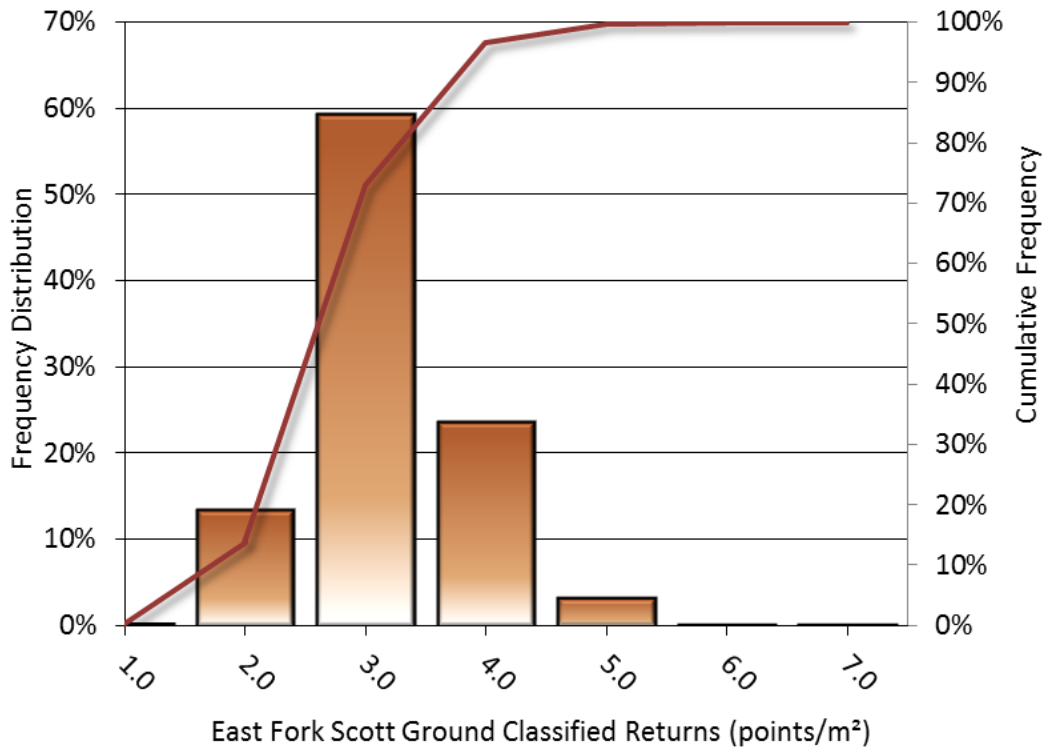


Figure 21: Frequency distribution of ground return densities per 100 m x 100 m cell

Lower Elk Creek AOI:

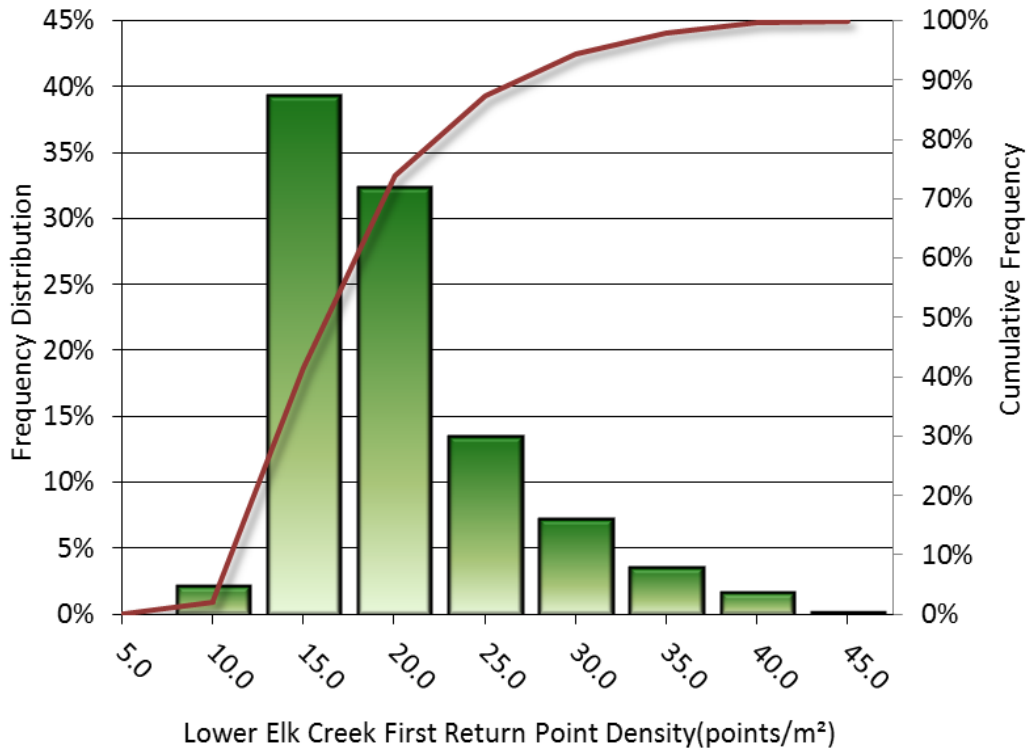


Figure 22: Frequency distribution of first return densities per 100 m x 100 m cell

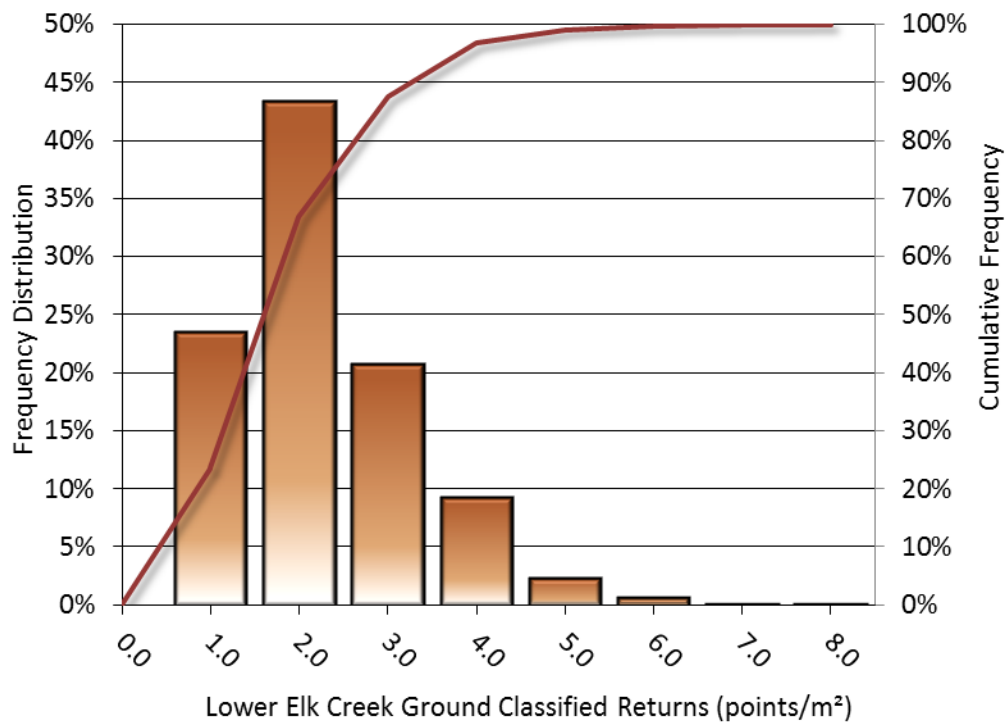


Figure 23: Frequency distribution of ground return densities per 100 m x 100 m cell

Pendola AOI:

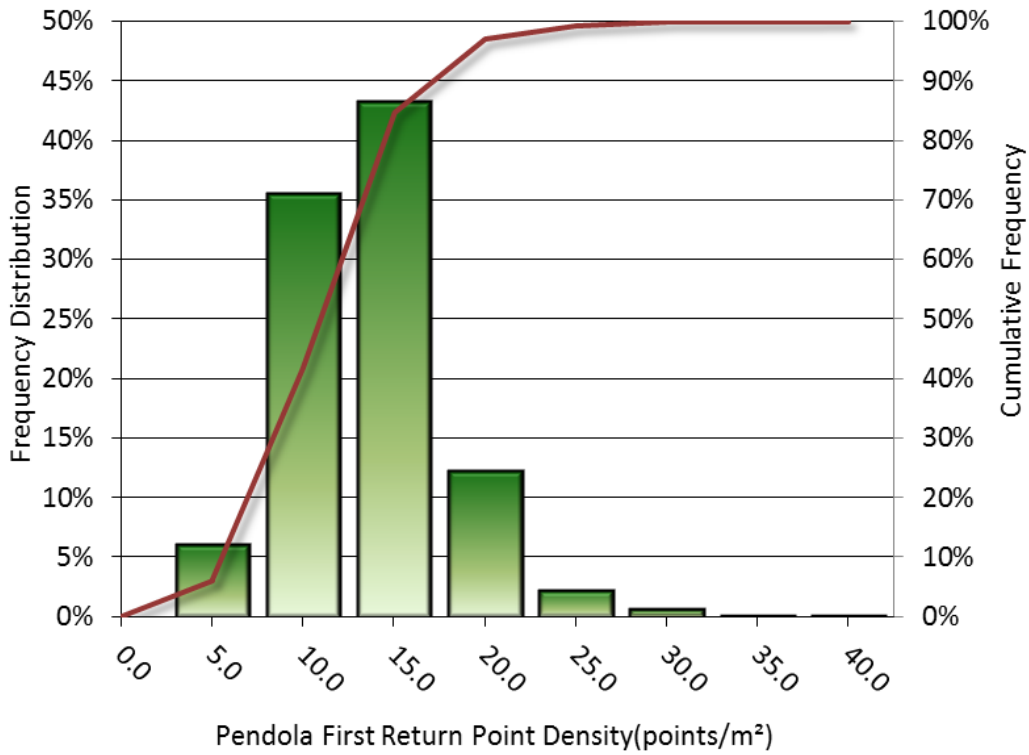


Figure 24: Frequency distribution of first return densities per 100 m x 100 m cell

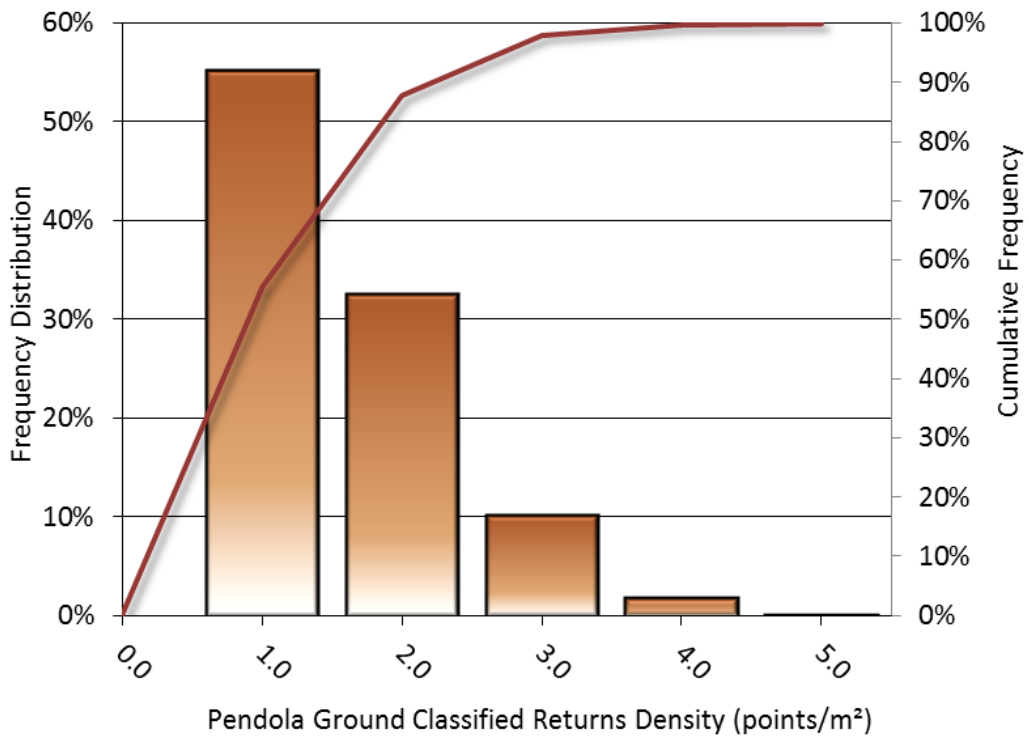


Figure 25: Frequency distribution of ground return densities per 100 m x 100 m cell

Squaw Creek AOI:

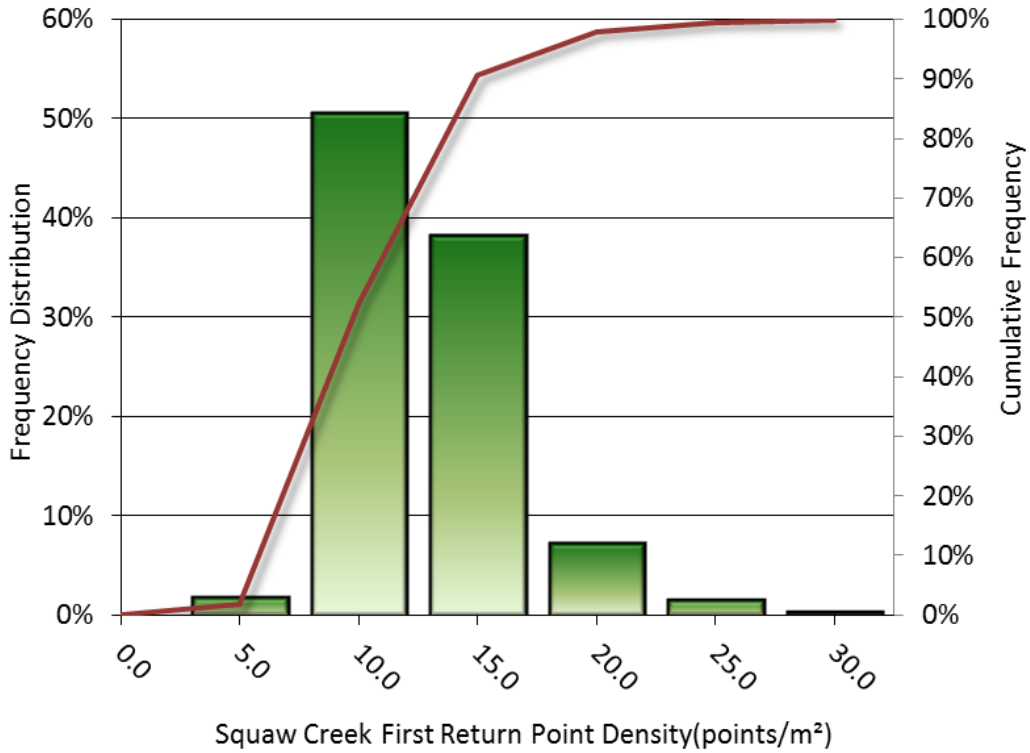


Figure 26: Frequency distribution of first return densities per 100 m x 100 m cell

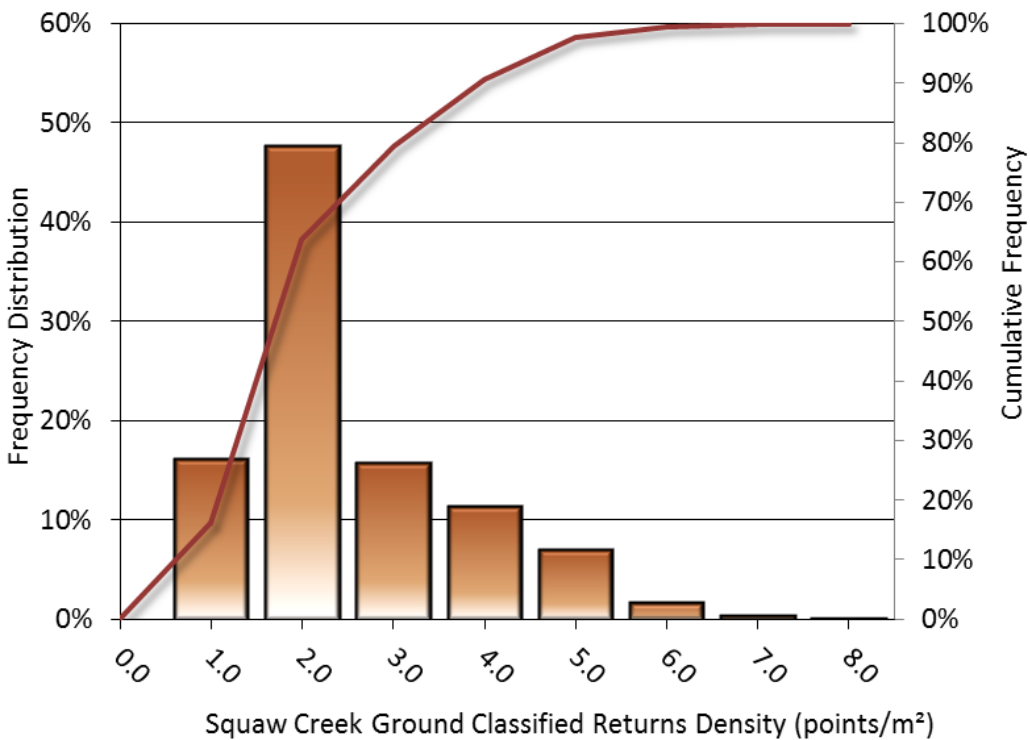


Figure 27: Frequency distribution of ground return densities per 100 m x 100 m cell

ST Experimental Forest AOI:

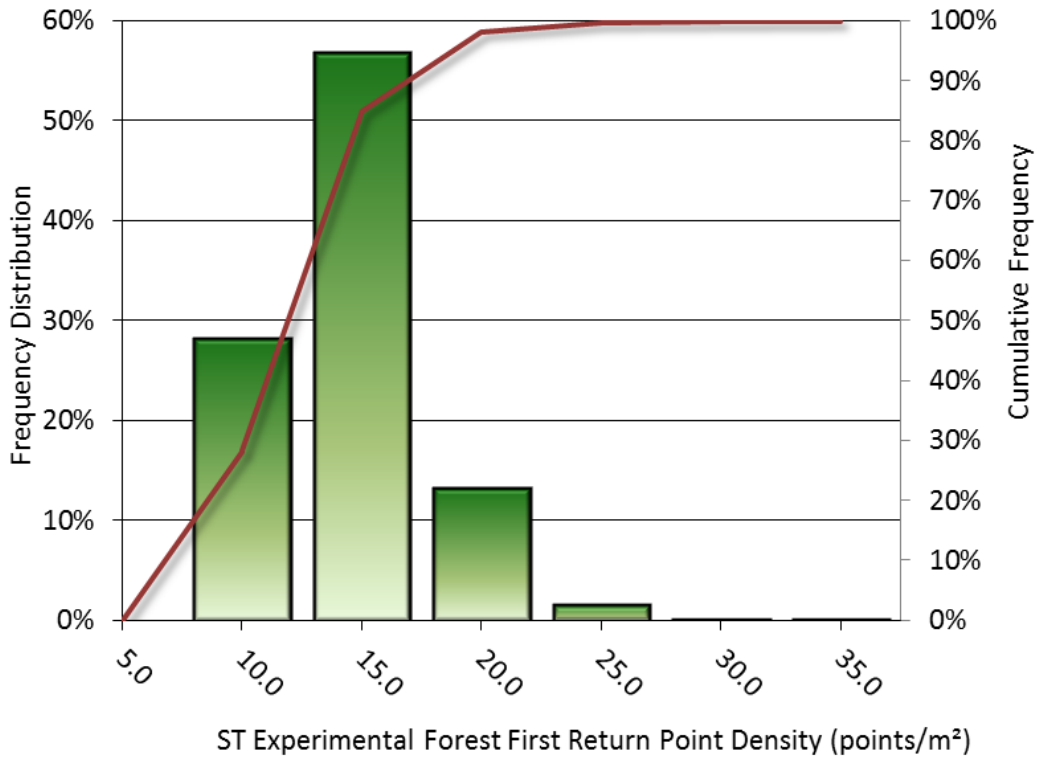


Figure 28: Frequency distribution of first return densities per 100 m x 100 m cell

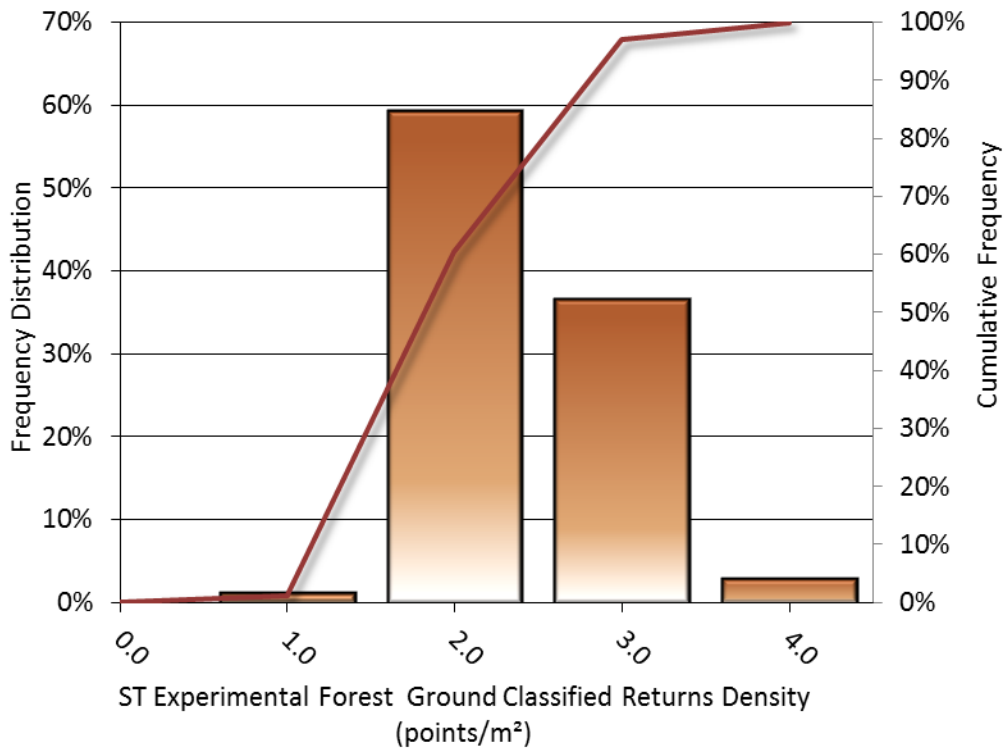


Figure 29: Frequency distribution of ground return densities per 100 m x 100 m cell

Sugar Creek AOI:

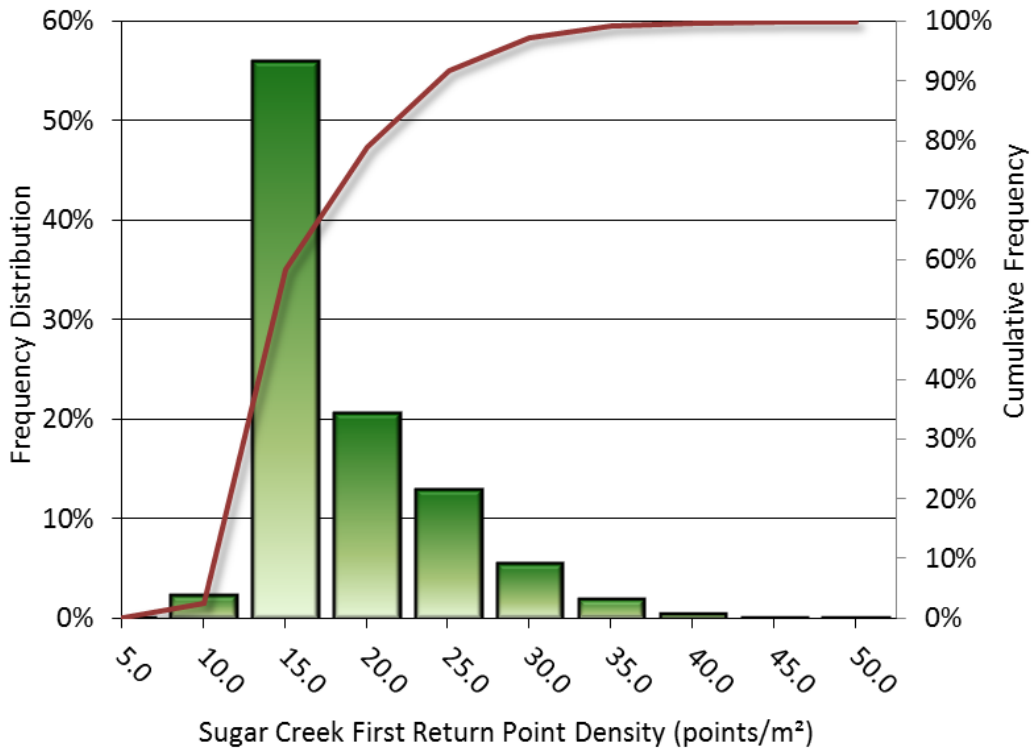


Figure 30: Frequency distribution of first return densities per 100 m x 100 m cell

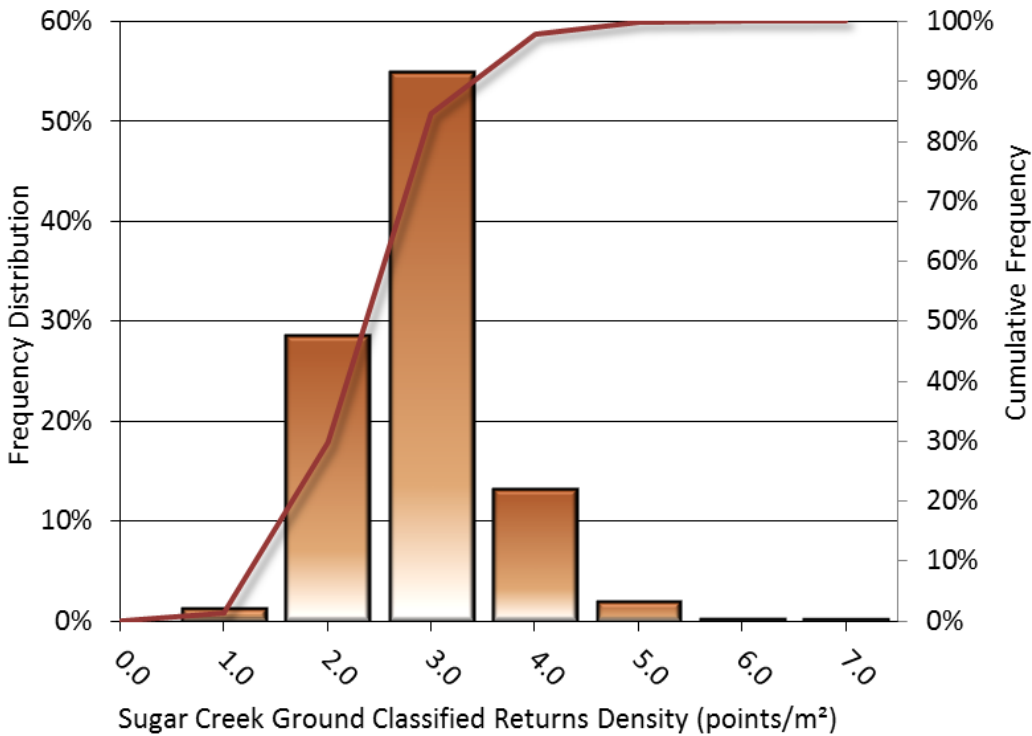


Figure 31: Frequency distribution of ground return densities per 100 m x 100 m cell

Van Vleck Meadows AOI:

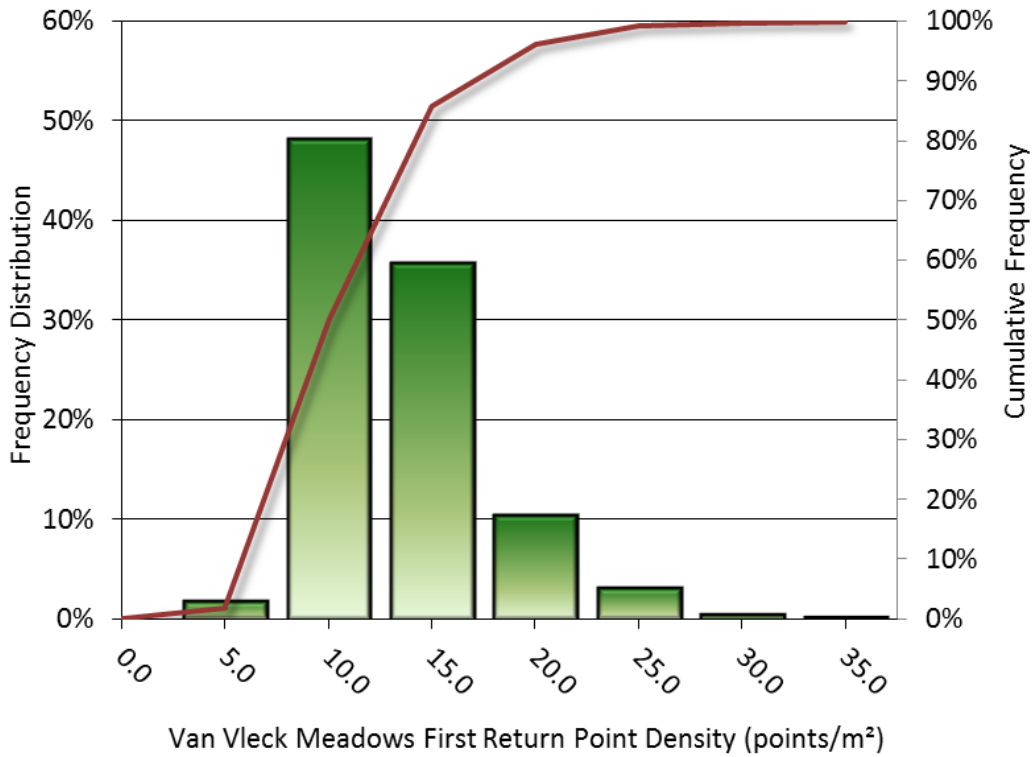


Figure 32: Frequency distribution of first return densities per 100 m x 100 m cell

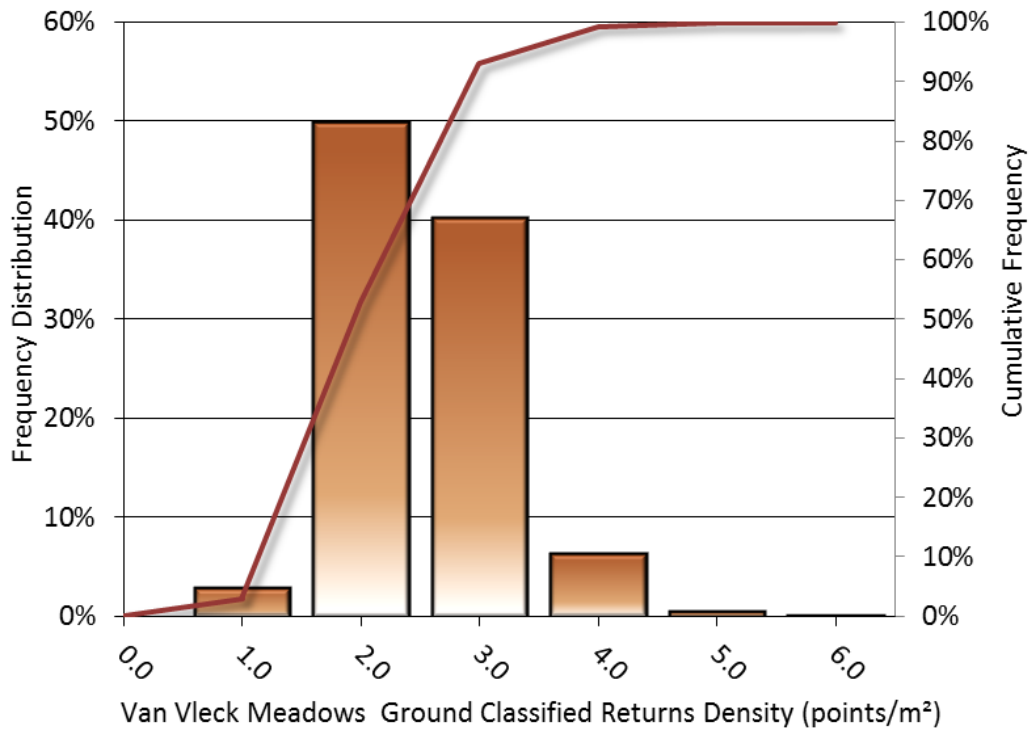


Figure 33: Frequency distribution of ground return densities per 100 m x 100 m cell

Freds Fire AOI:

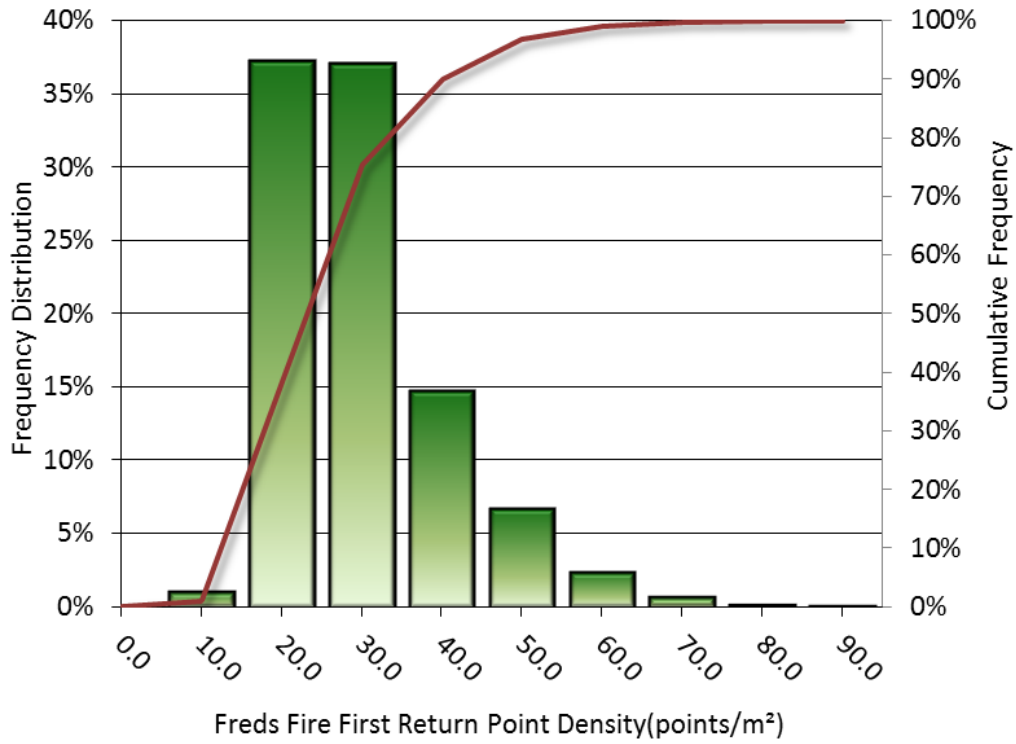


Figure 34: Frequency distribution of first return densities per 100 m x 100 m cell

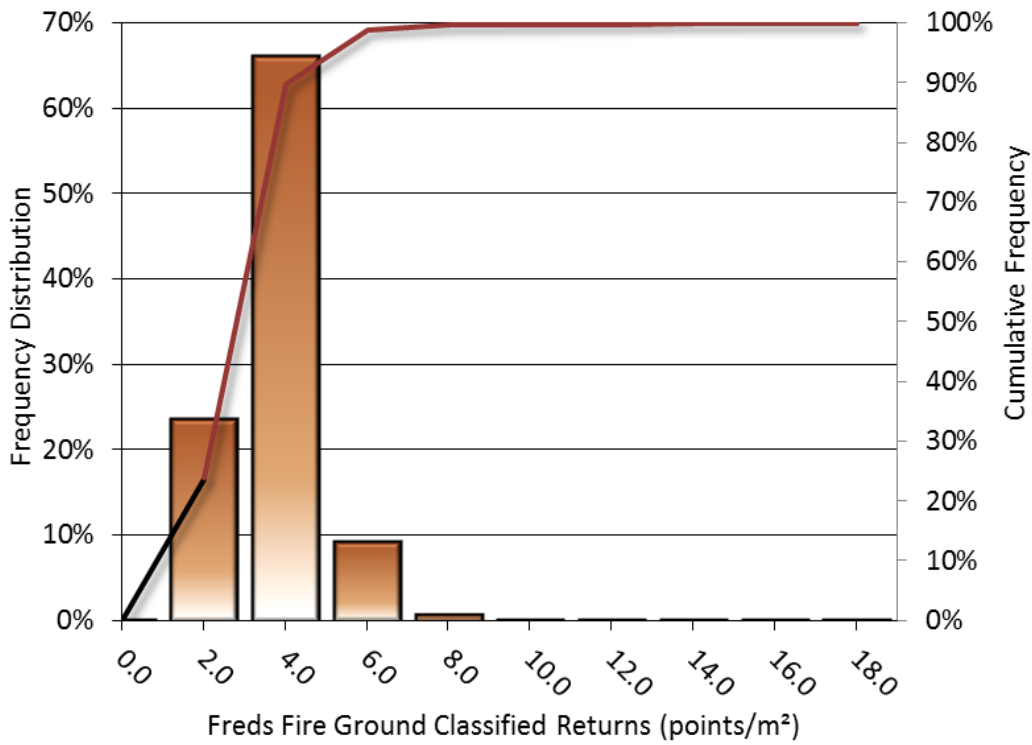


Figure 35: Frequency distribution of ground return densities per 100 m x 100 m cell

Power Fire AOI:

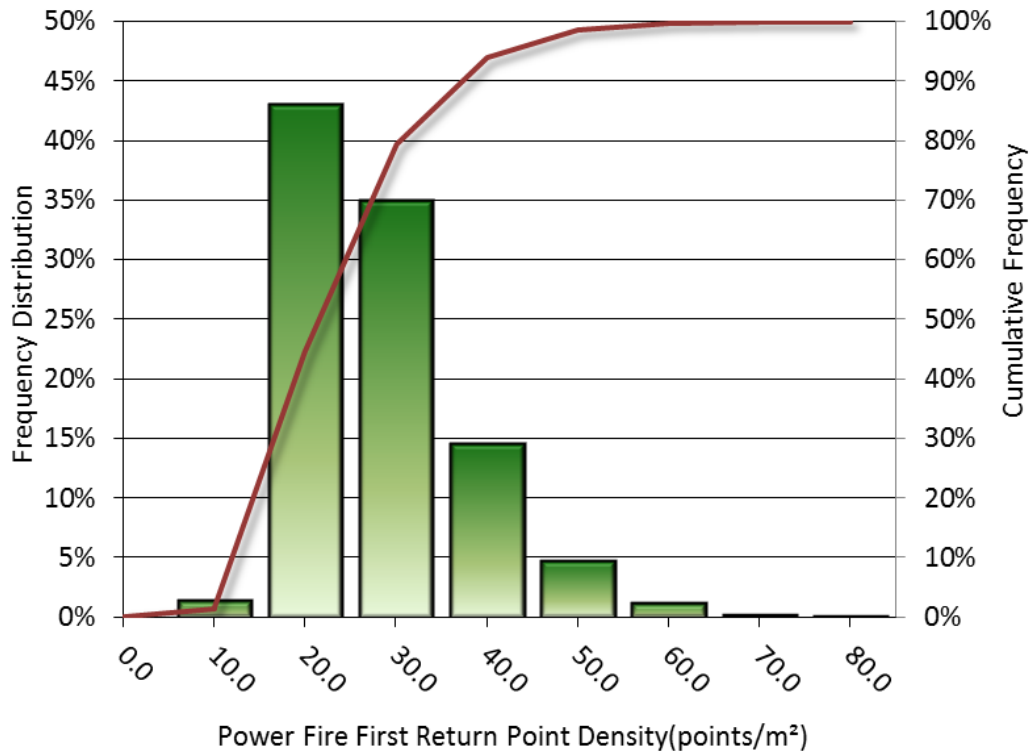


Figure 36: Frequency distribution of first return densities per 100 m x 100 m cell

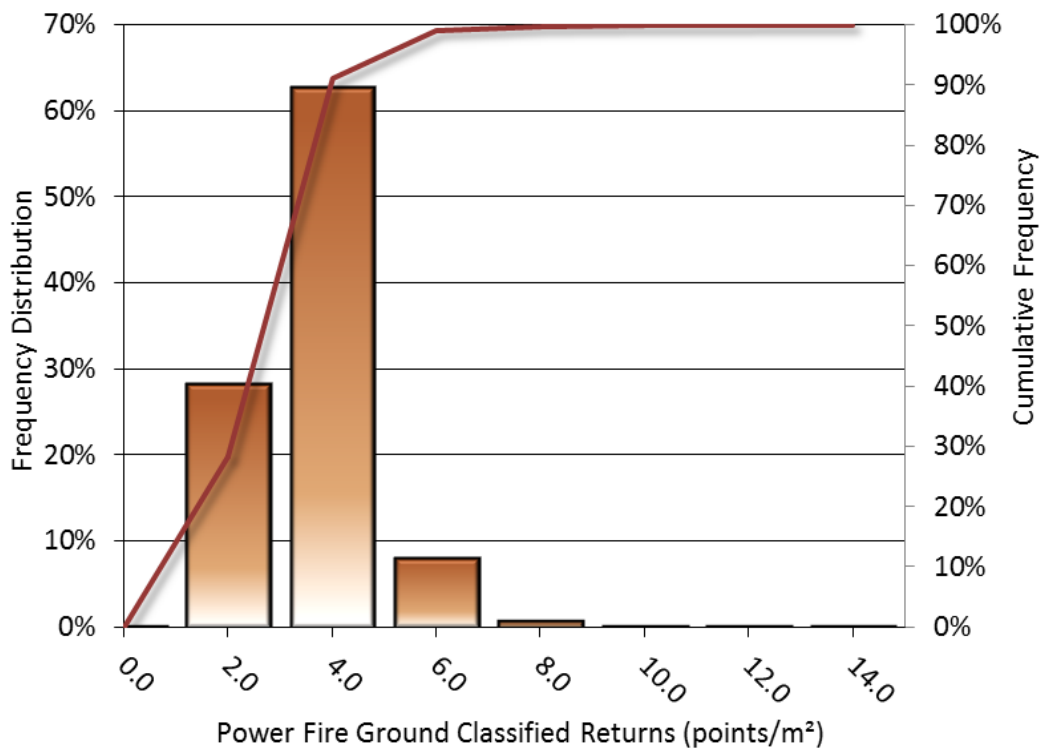


Figure 37: Frequency distribution of ground return densities per 100 m x 100 m cell

APPENDIX C: ABSOLUTE ACCURACY RESULTS

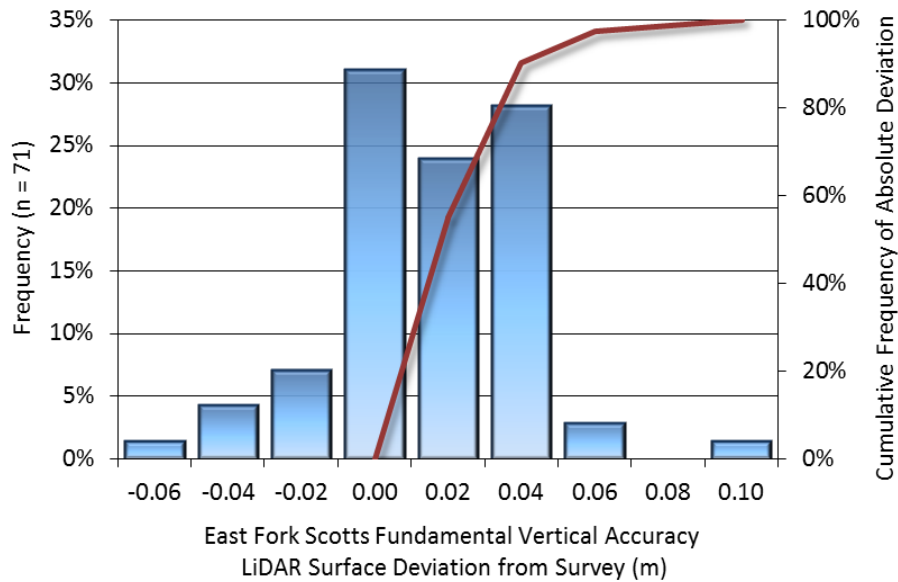


Figure 38: Frequency histogram for LiDAR surface deviation from ground check point values in the East Forks Scott River AOI

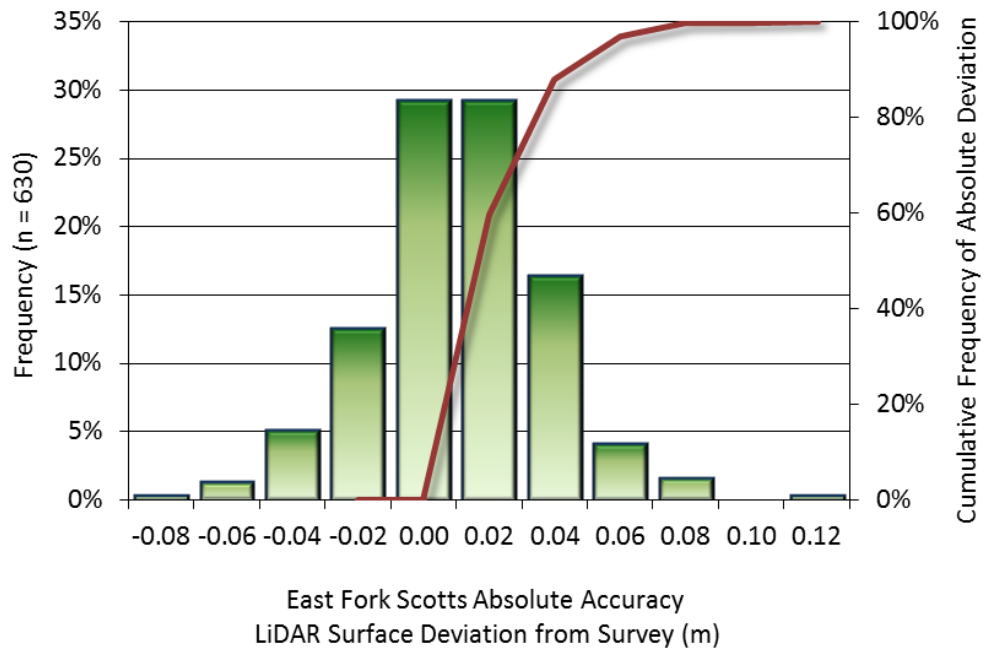


Figure 39: Frequency histogram for LiDAR surface deviation from ground control point values in the East Forks Scott River AOI

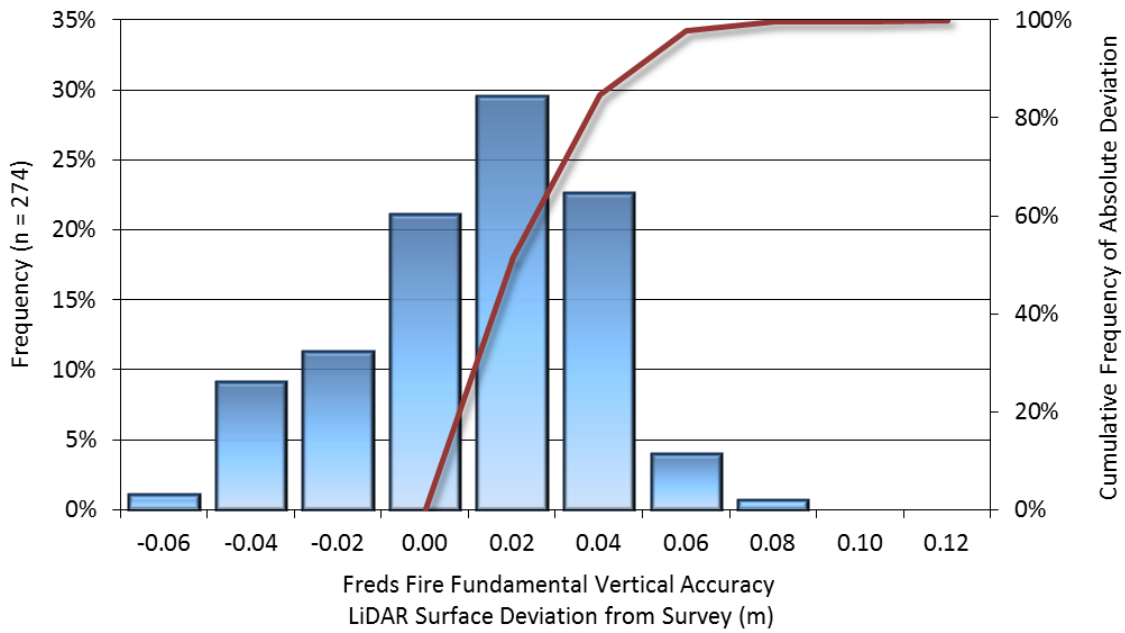


Figure 40: Frequency histogram for LiDAR surface deviation from ground check point values in the Freds Fire AOI

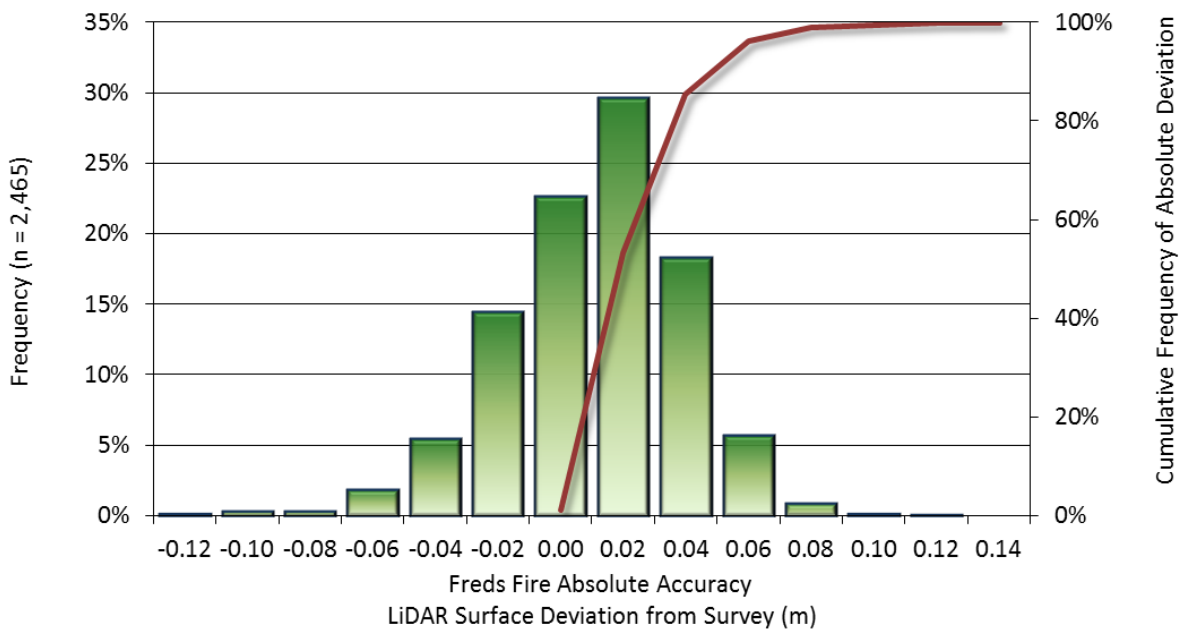


Figure 41: Frequency histogram for LiDAR surface deviation from ground control point values in the Freds Fire AOI

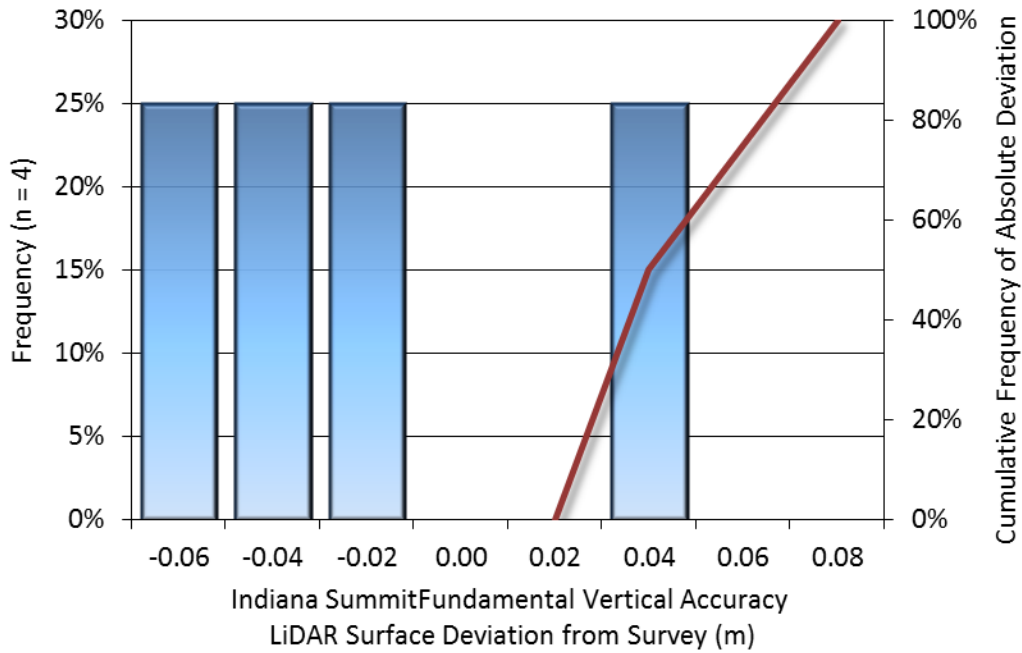


Figure 42: Frequency histogram for LiDAR surface deviation from ground check point values in the Indiana Summit AOI

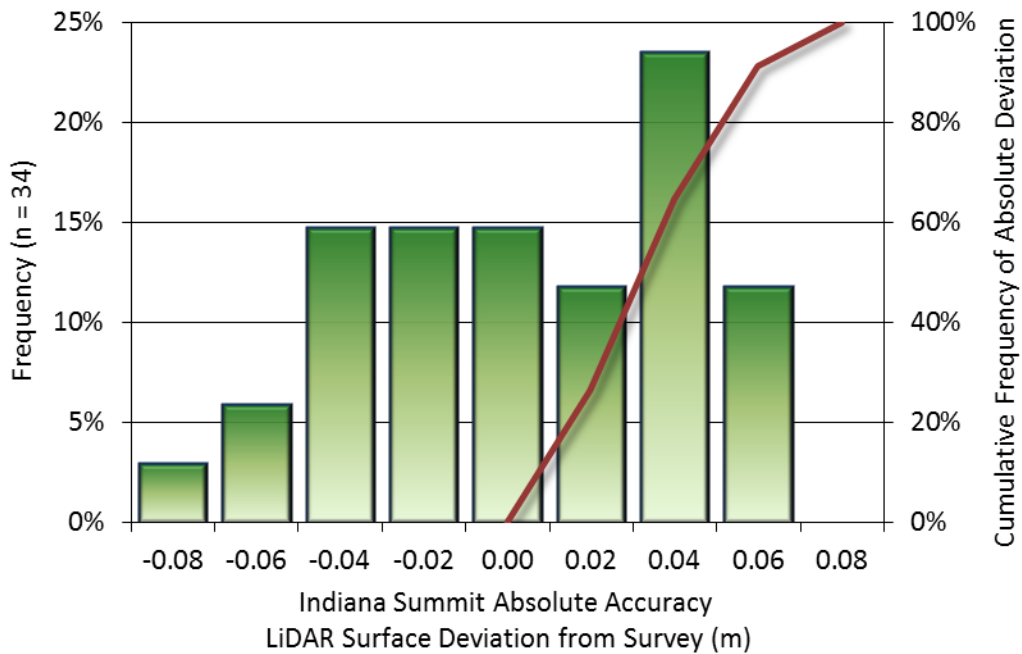


Figure 43: Frequency histogram for LiDAR surface deviation from ground control point values in the Indiana Summit AOI

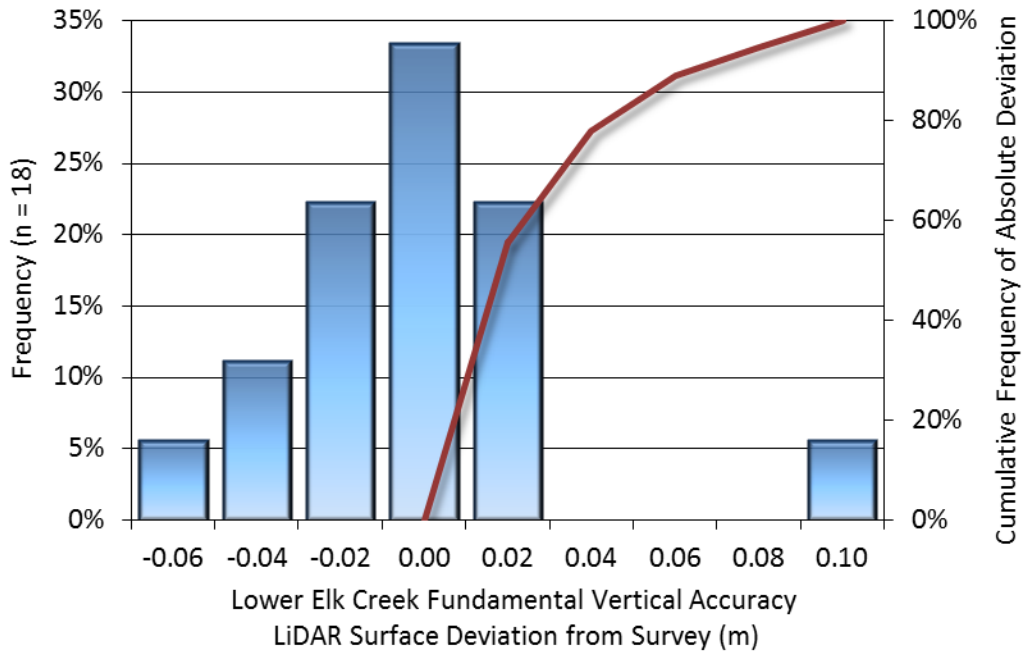


Figure 44: Frequency histogram for LiDAR surface deviation from ground check point values in the Lower Elk Creek AOI

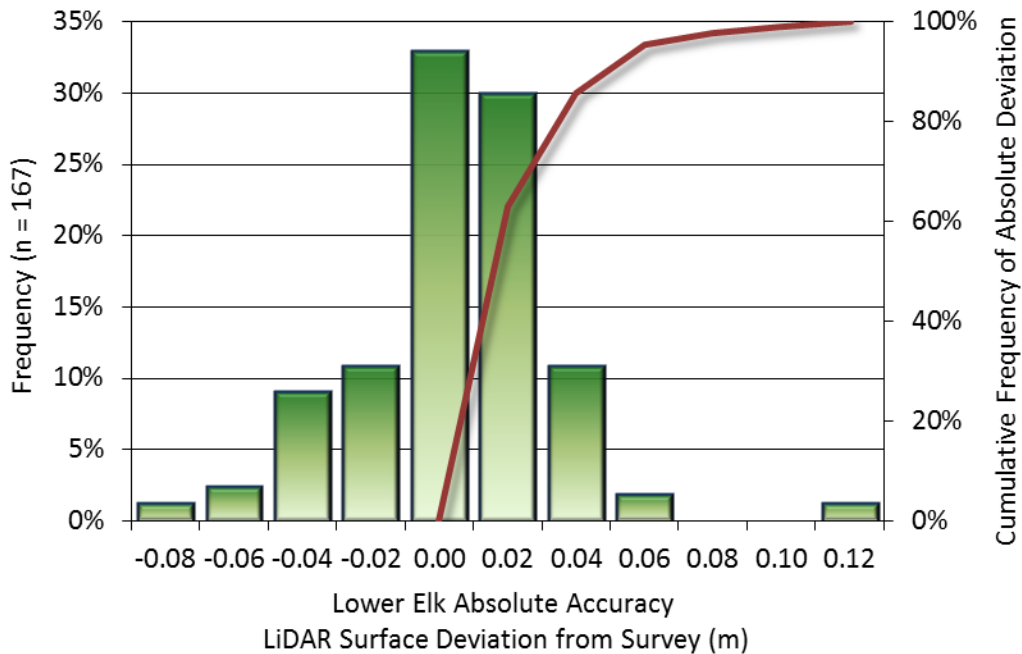


Figure 45: Frequency histogram for LiDAR surface deviation from ground control point values in the Lower Elk Creek AOI

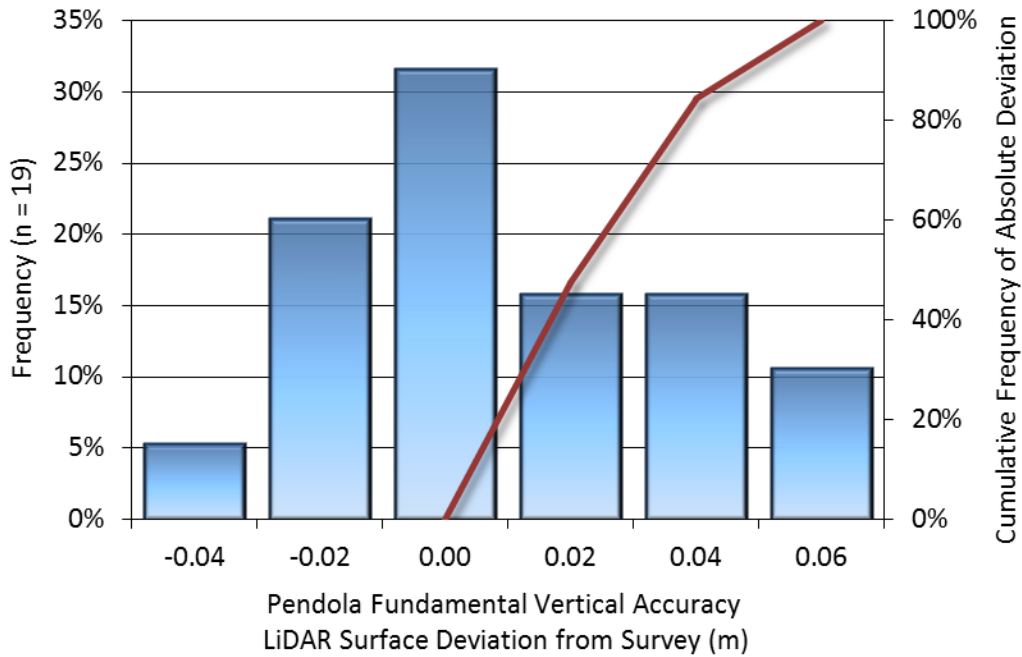


Figure 46: Frequency histogram for LiDAR surface deviation from ground check point values in the Pendola AOI

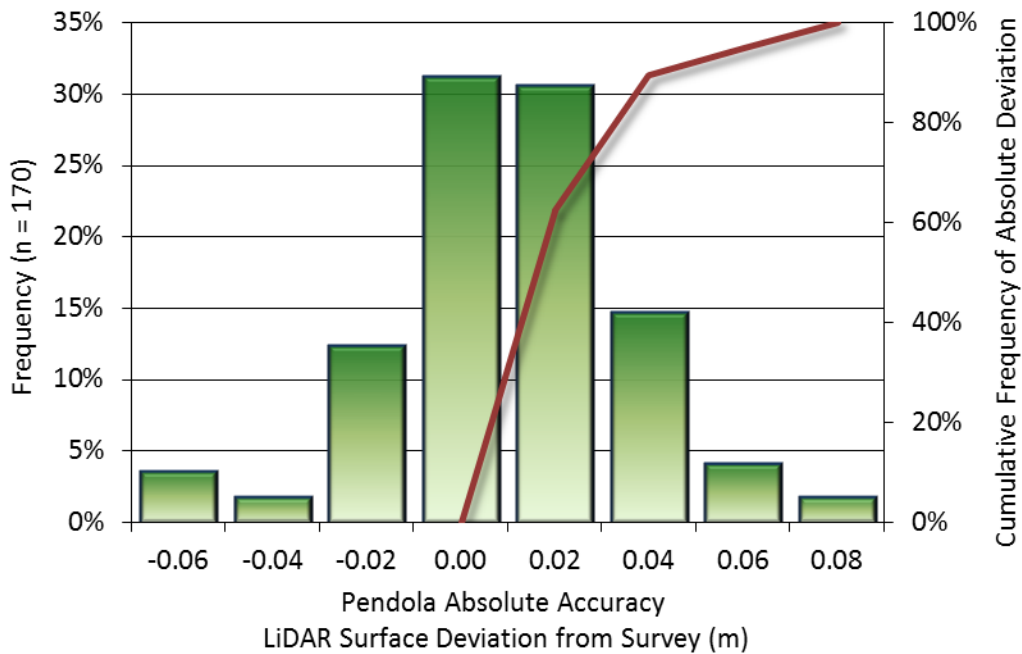


Figure 47: Frequency histogram for LiDAR surface deviation from ground control point values in the Pendola AOI

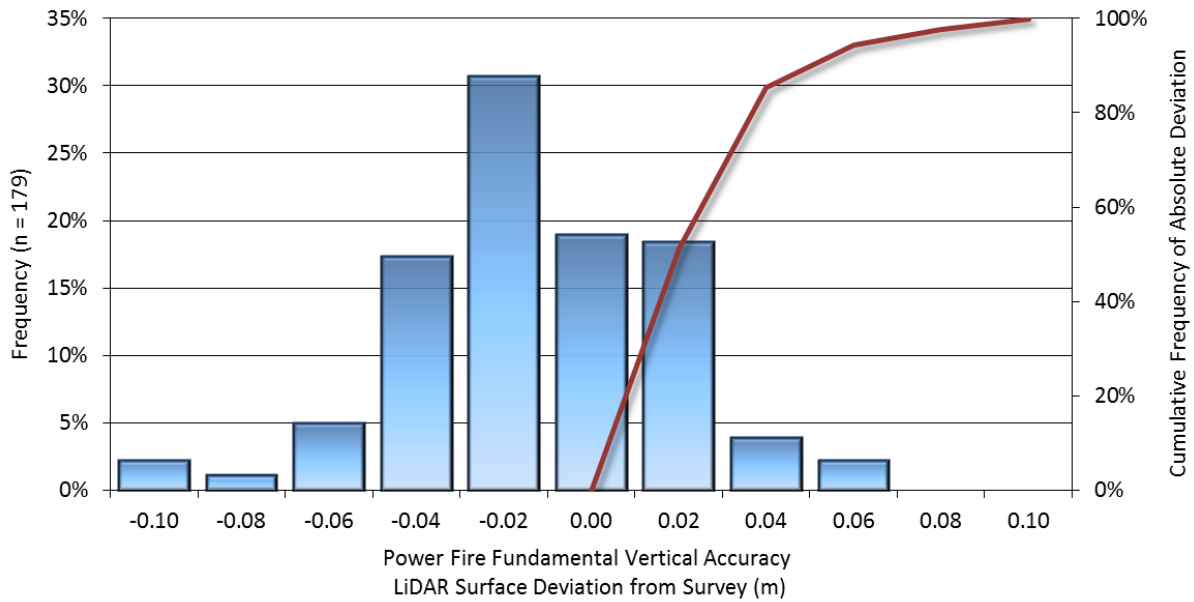


Figure 48: Frequency histogram for LiDAR surface deviation from ground check point values in the Power Fire AOI

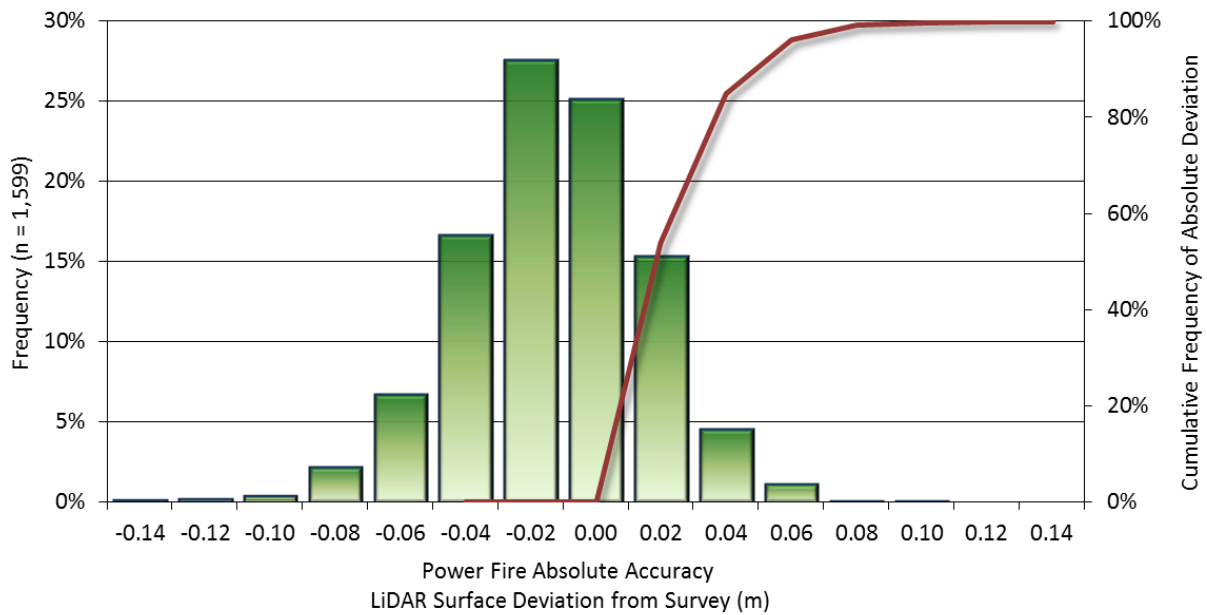


Figure 49: Frequency histogram for LiDAR surface deviation from ground control point values in the Power Fire AOI

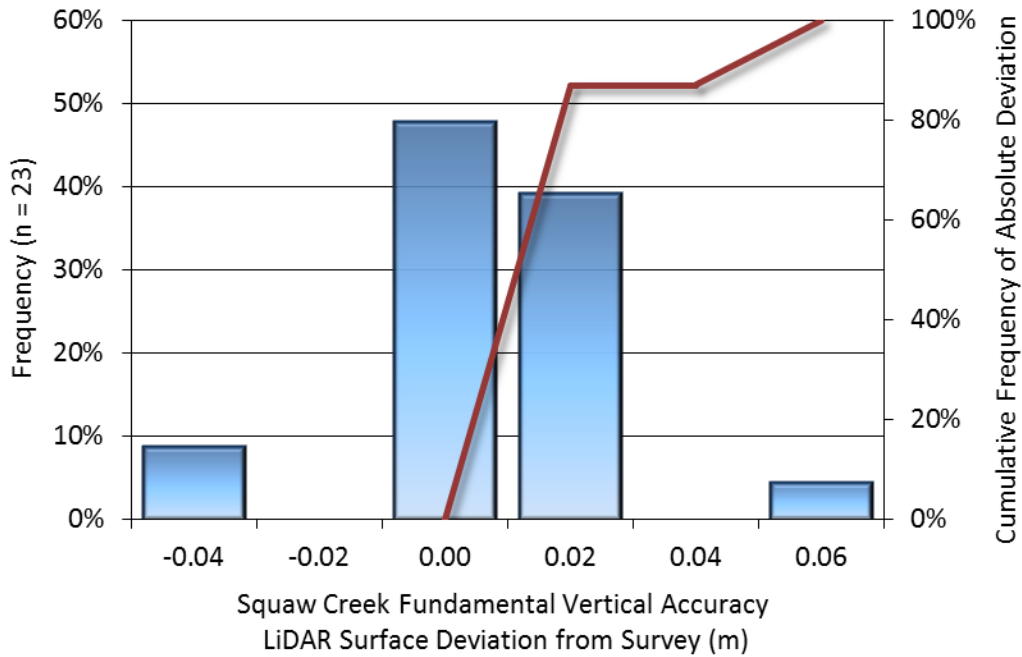


Figure 50: Frequency histogram for LiDAR surface deviation from ground check point values in the Squaw Creek AOI

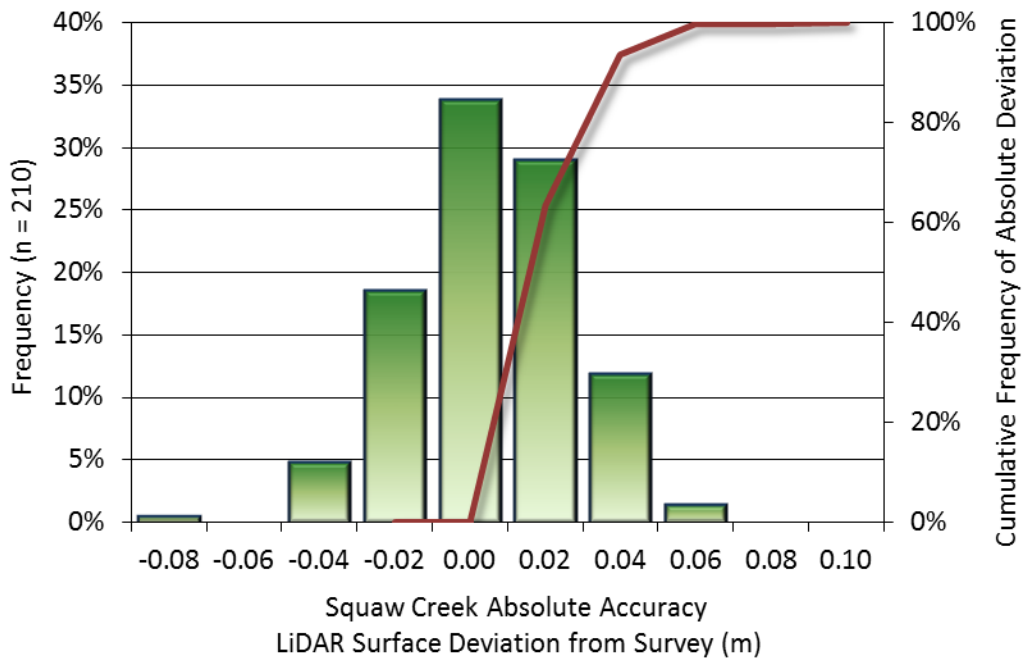


Figure 51: Frequency histogram for LiDAR surface deviation from ground control point values in the Squaw Creek AOI

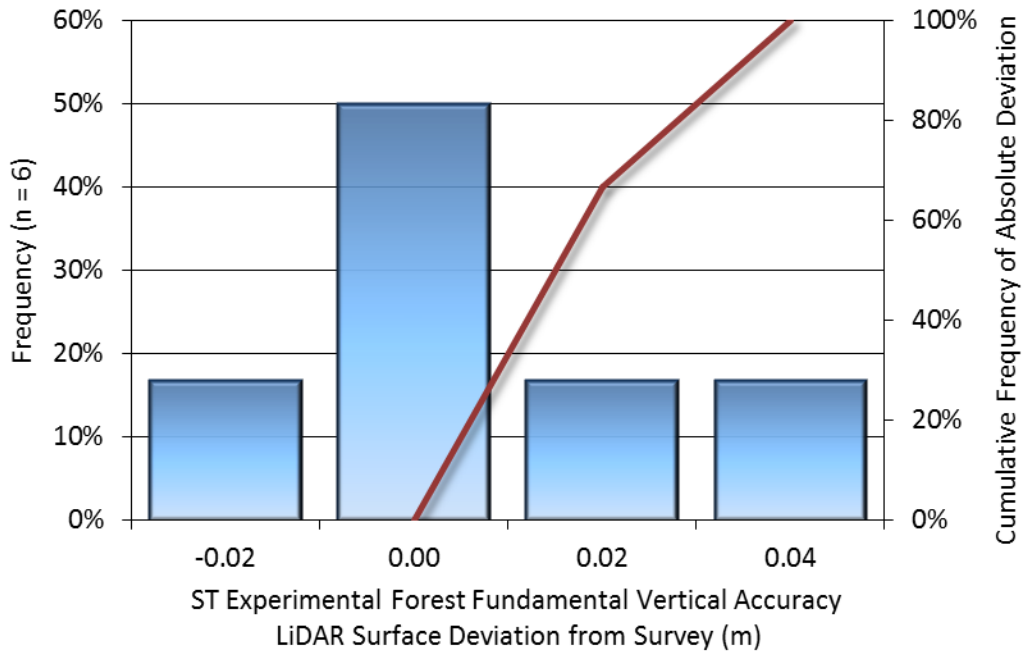


Figure 52: Frequency histogram for LiDAR surface deviation from ground check point values in the ST Experimental Forest AOI

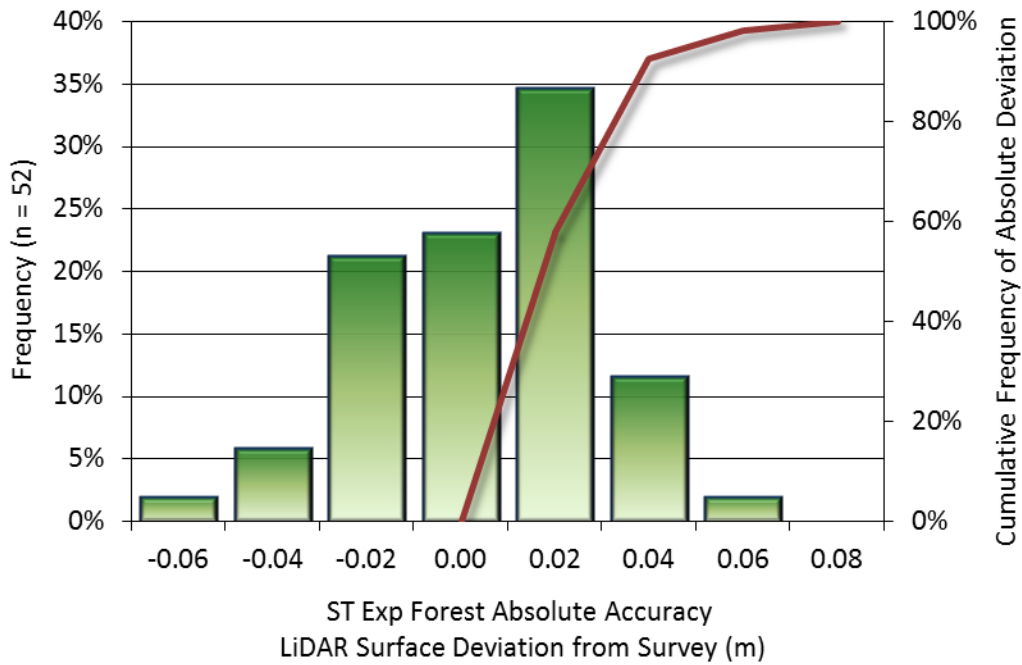


Figure 53: Frequency histogram for LiDAR surface deviation from ground check point values in the ST Experimental Forest AOI

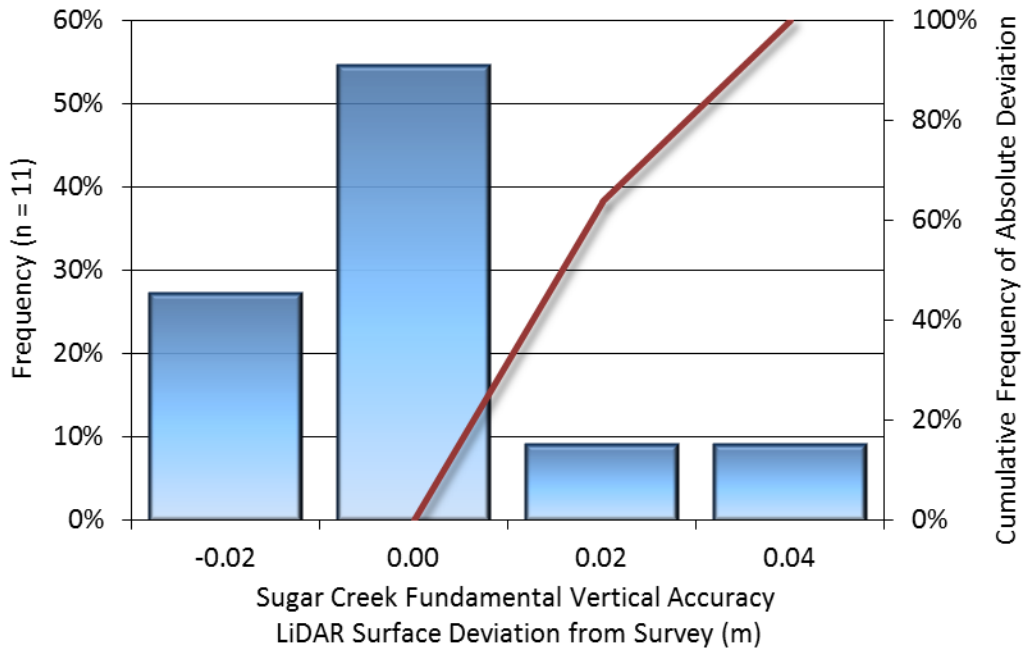


Figure 54: Frequency histogram for LiDAR surface deviation from ground check point values in the Sugar Creek AOI

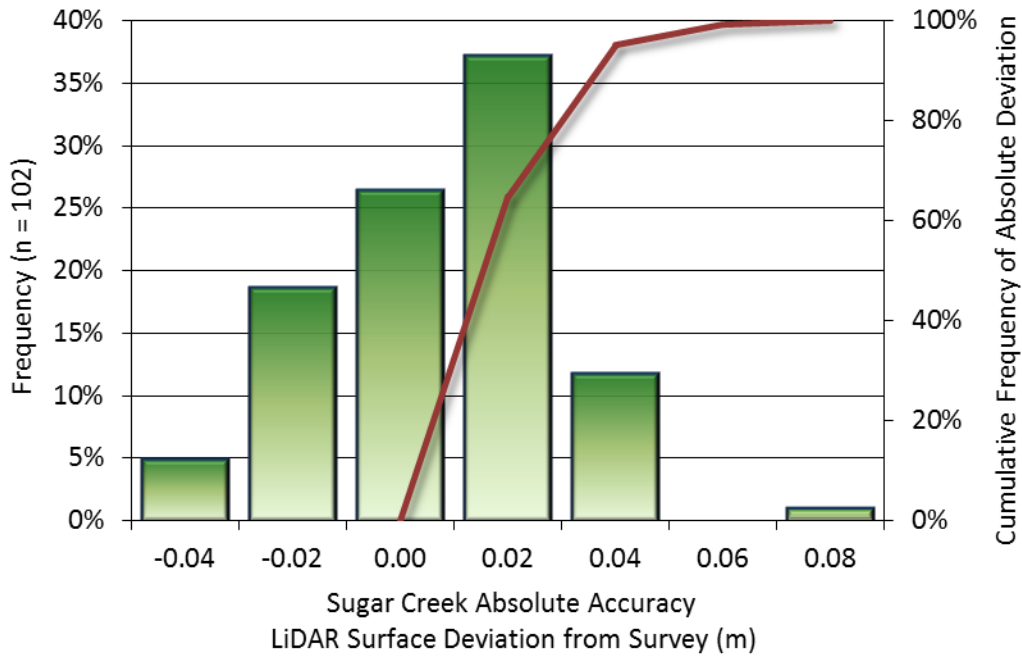


Figure 55: Frequency histogram for LiDAR surface deviation from ground check point values in the Sugar Creek AOI

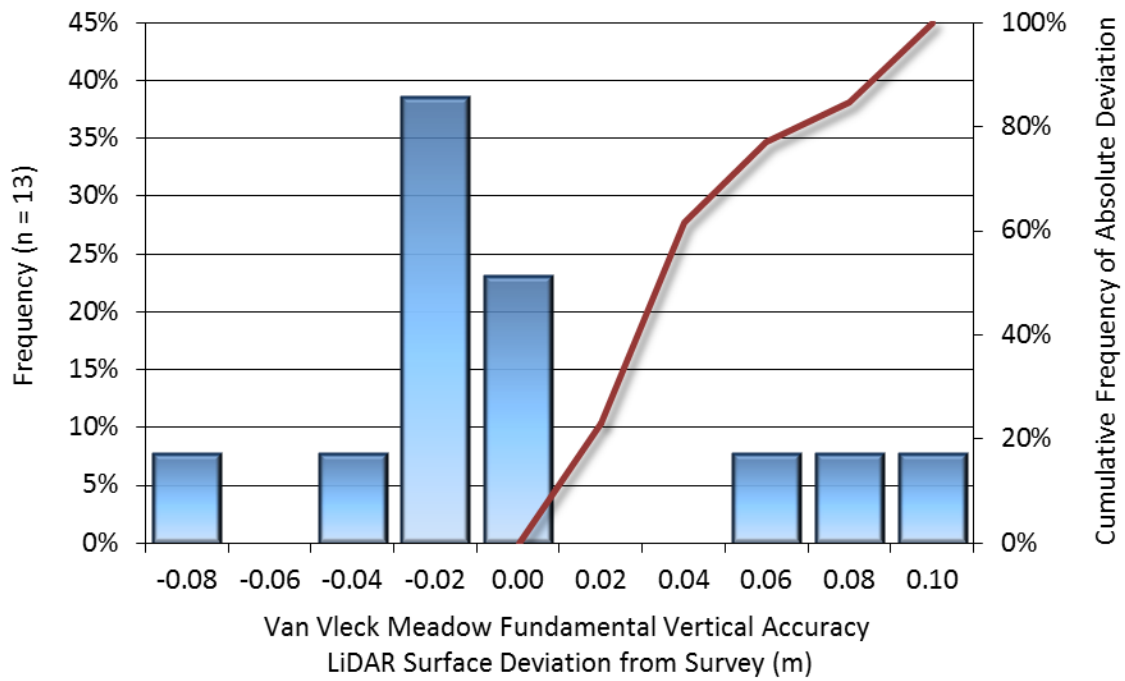


Figure 56: Frequency histogram for LiDAR surface deviation from ground check point values in the Van Vleck Meadow AOI

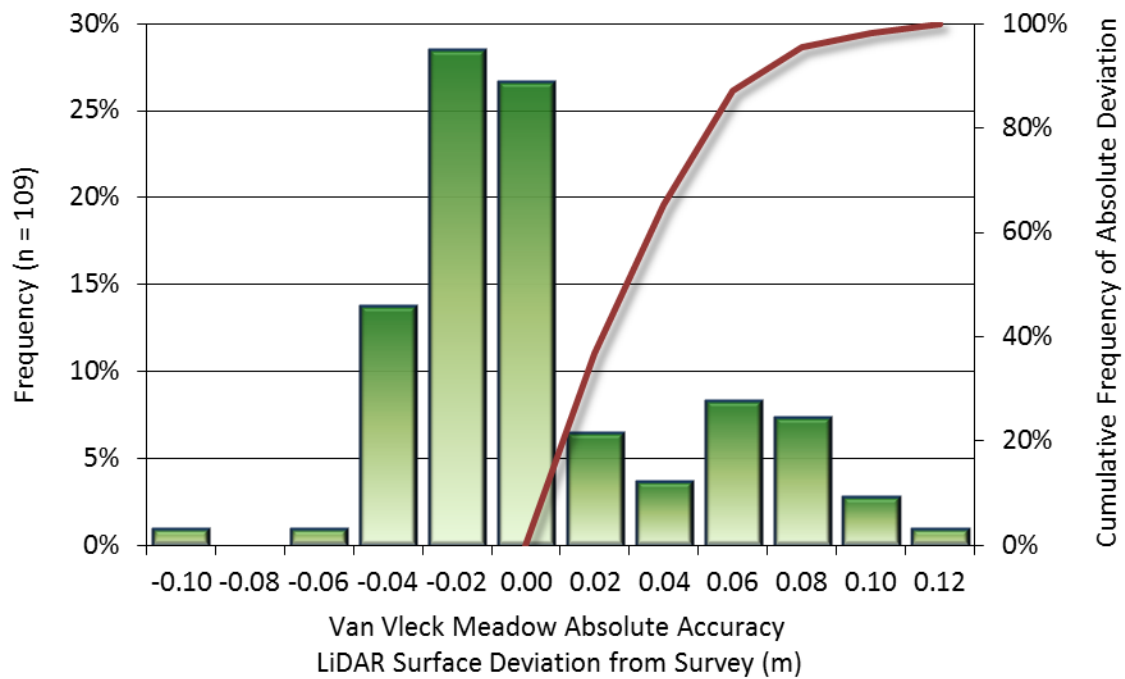


Figure 57: Frequency histogram for LiDAR surface deviation from ground check point values in the Van Vleck Meadow AOI

APPENDIX D: RELATIVE ACCURACY RESULTS

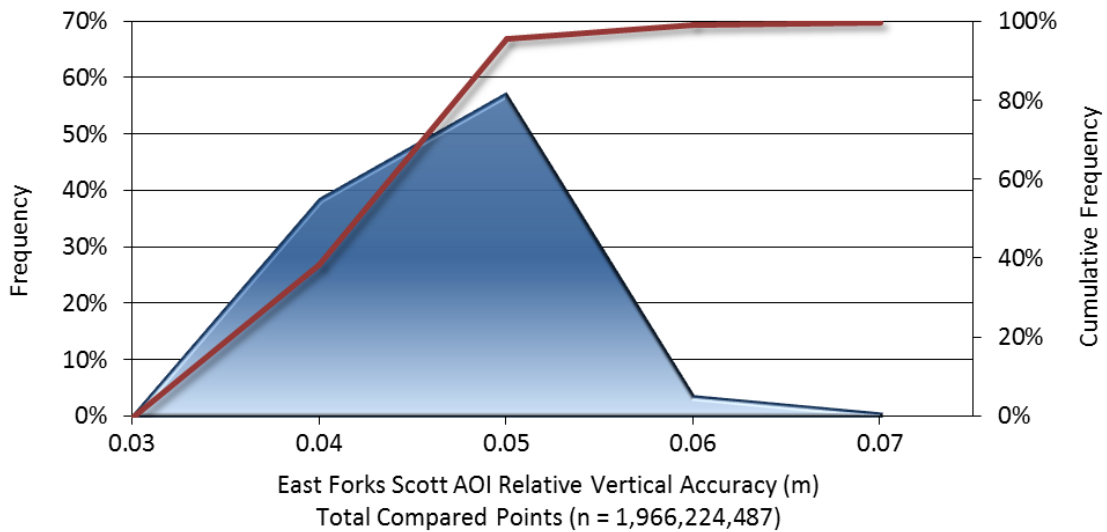


Figure 58: Frequency plot for relative vertical accuracy between flight lines in the East Forks Scott River AOI

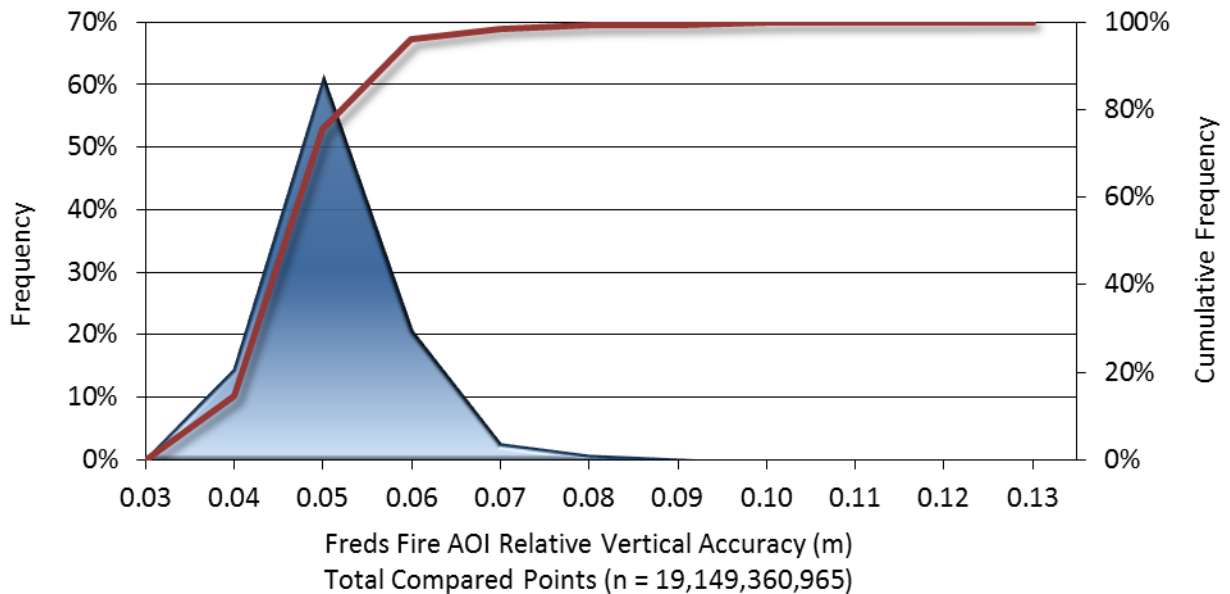


Figure 59: Frequency plot for relative vertical accuracy between flight lines in the Freds Fire AOI

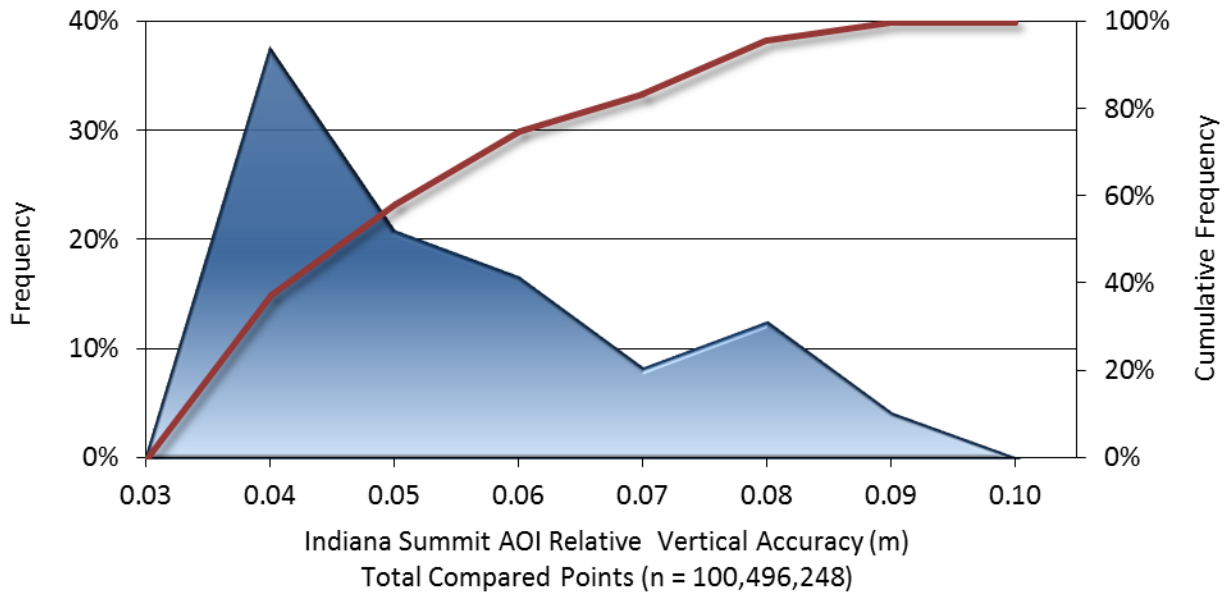


Figure 60: Frequency plot for relative vertical accuracy between flight lines in the Indiana Summit AOI

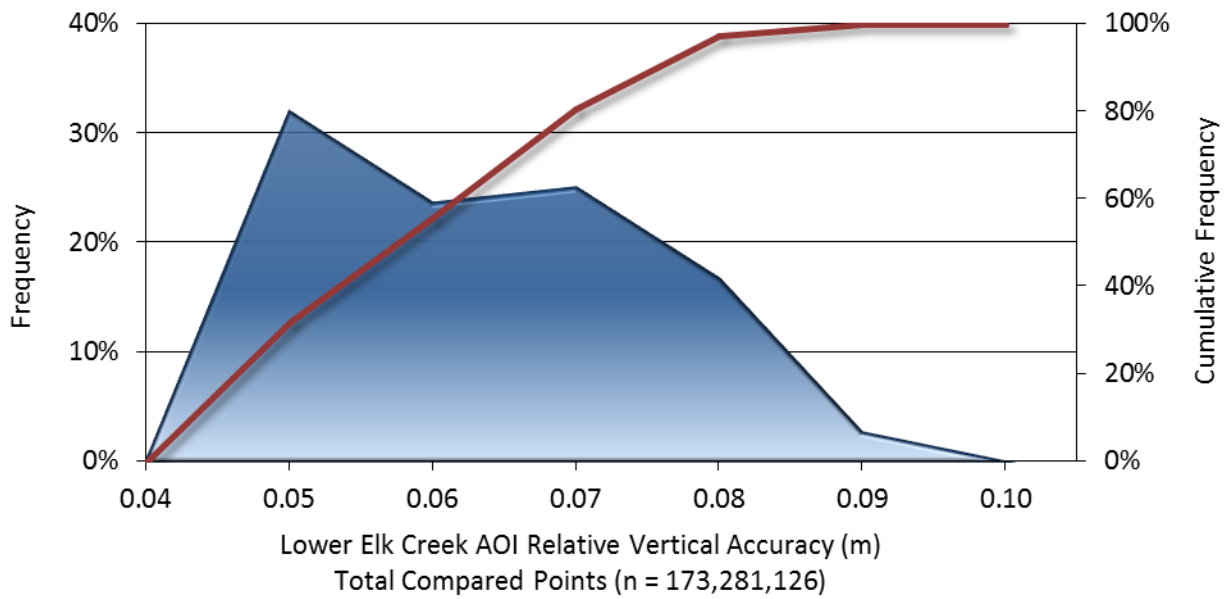


Figure 61: Frequency plot for relative vertical accuracy between flight lines in the Lower Elk Creek AOI

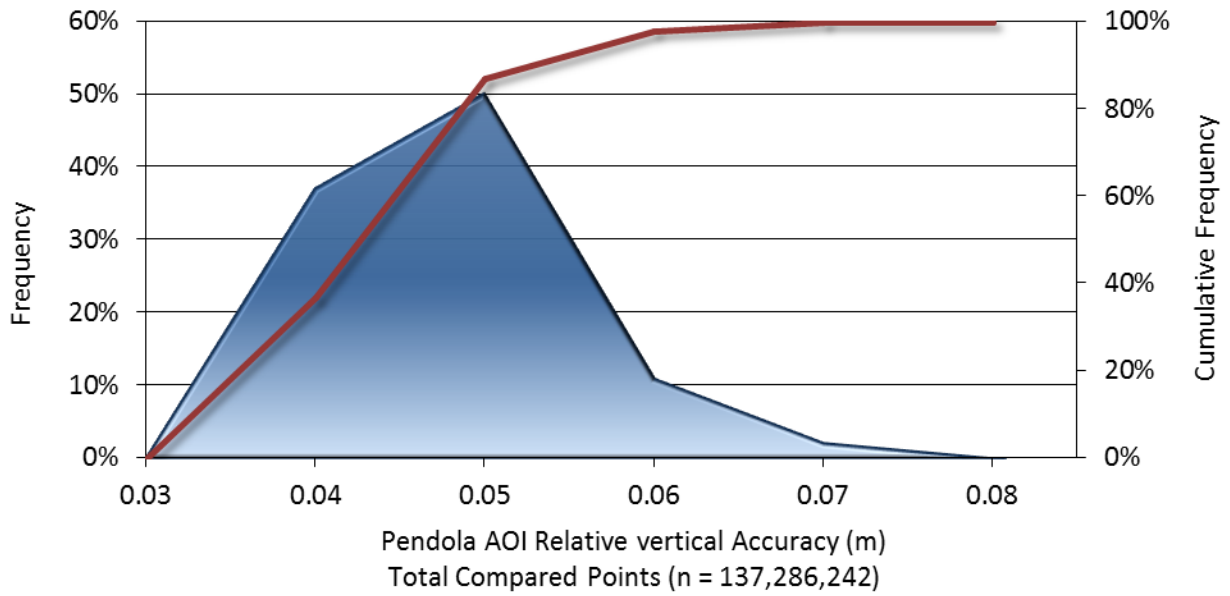


Figure 62: Frequency plot for relative vertical accuracy between flight lines in the Pendola AOI

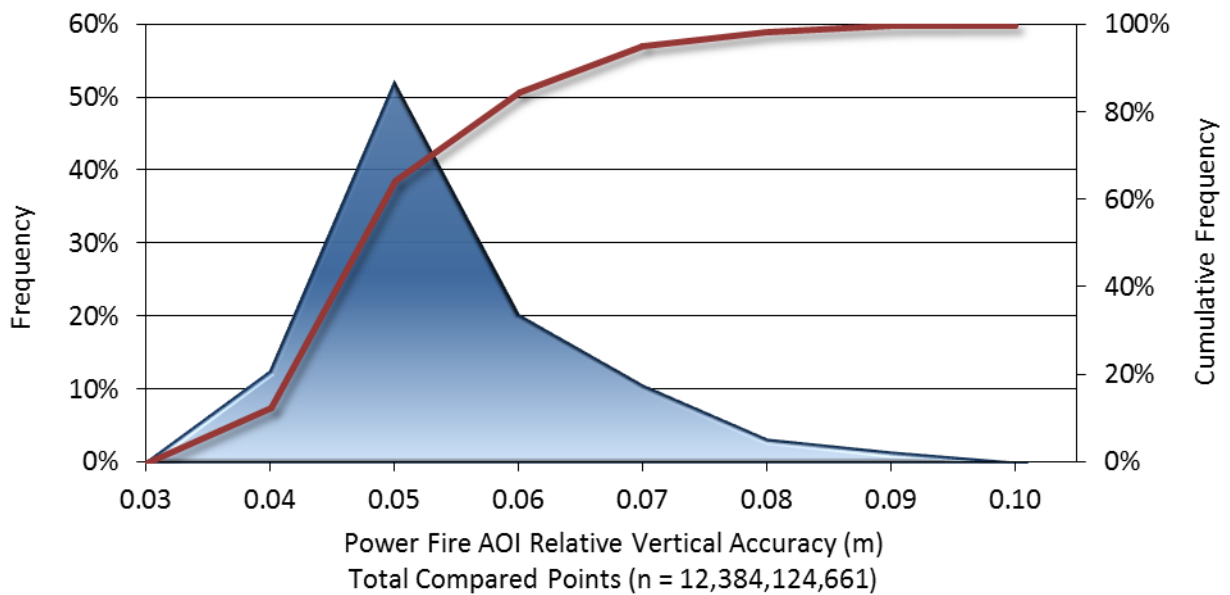


Figure 63: Frequency plot for relative vertical accuracy between flight lines in the Power Fire AOI

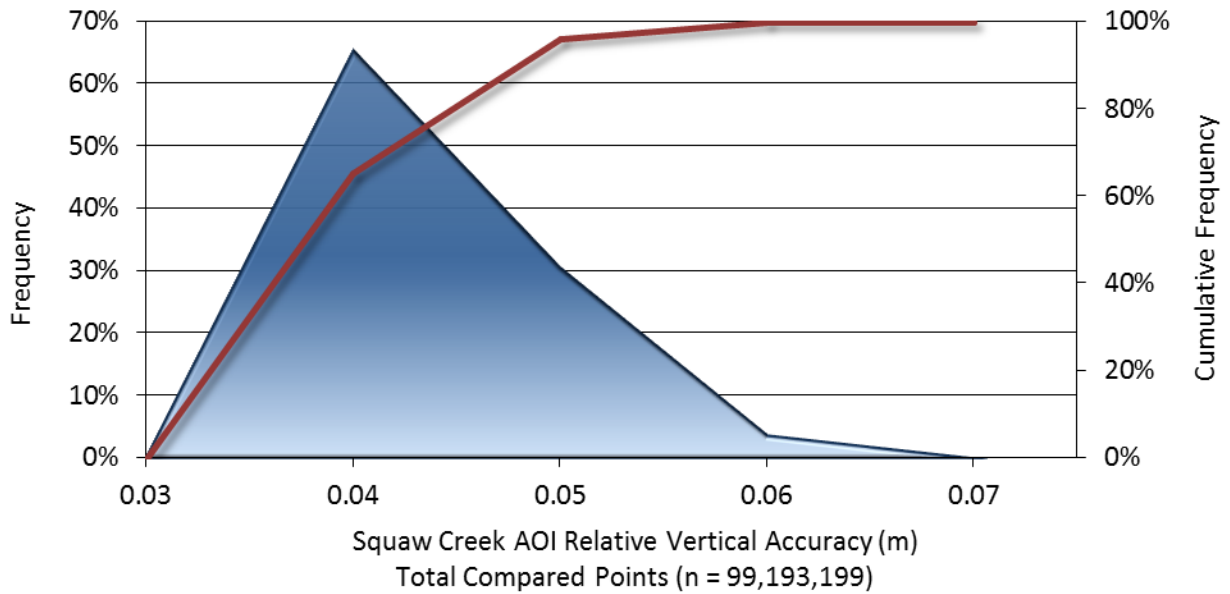


Figure 64: Frequency plot for relative vertical accuracy between flight lines in the Squaw Creek AOI

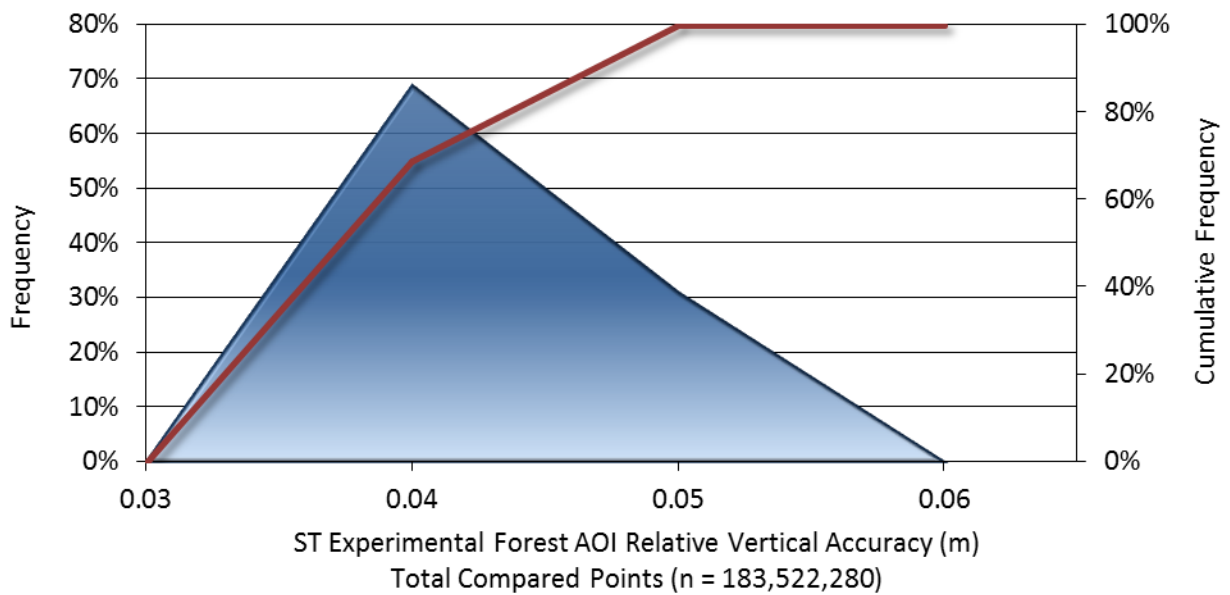


Figure 65: Frequency plot for relative vertical accuracy between flight lines in the ST Experimental Forest AOI

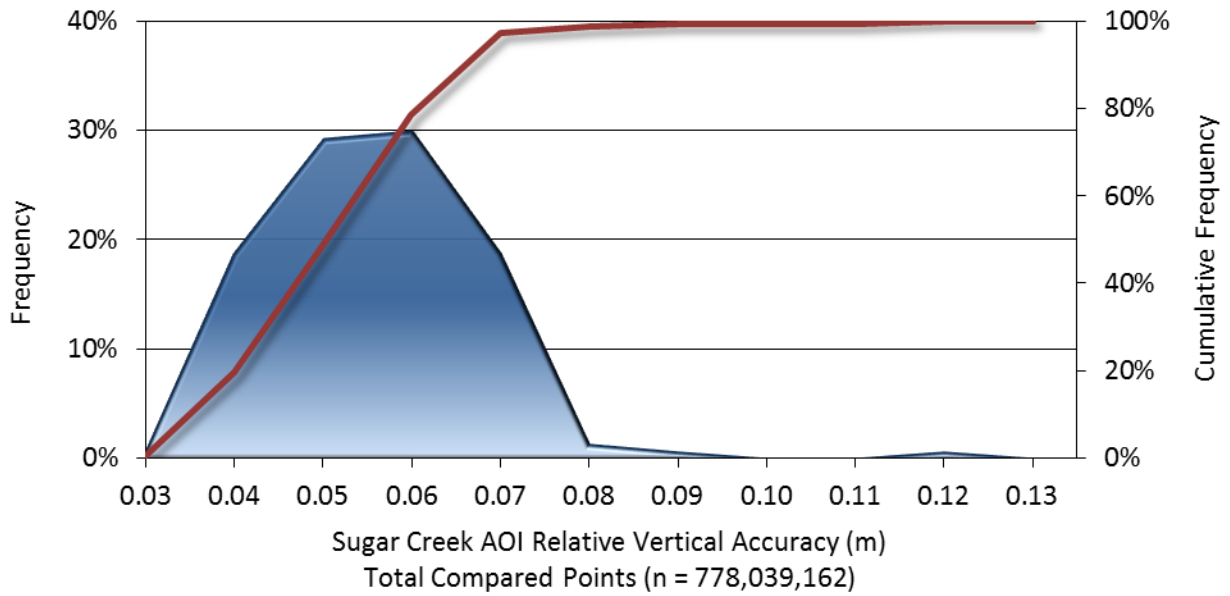


Figure 66: Frequency plot for relative vertical accuracy between flight lines in the Sugar Creek AOI

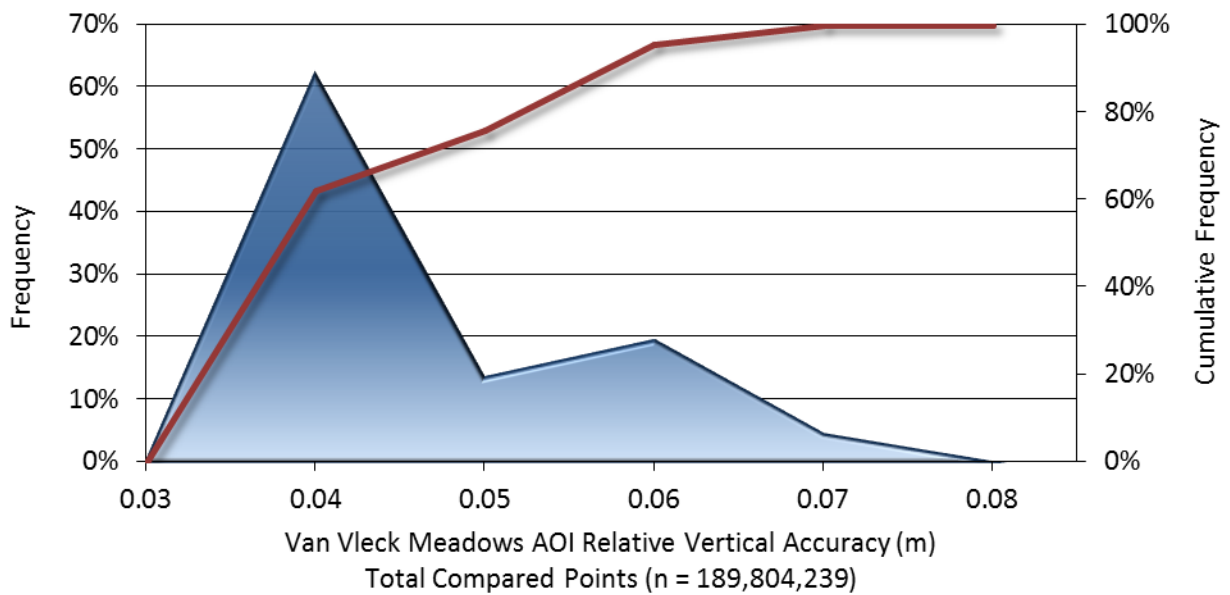


Figure 67: Frequency plot for relative vertical accuracy between flight lines in the Van Vleck Meadow AOI